J. Fluid Mech. (1992), *vol.* 241, *pp.* 669–704
Printed in Great Britain

Nonlinear dynamics in Langmuir circulations with $O(2)$ symmetry

By STEPHEN M. COX[1]†, SIDNEY LEIBOVICH[1], IRENE M. MOROZ[2] AND AMIT TANDON[1]

[1]Sibley School of Mechanical and Aerospace Engineering, Upson Hall, Cornell University, Ithaca, NY 14853-7501, USA

[2]School of Mathematics, University of East Anglia, Norwich NR4 7TJ, UK

(Received 15 October 1991 and in revised form 7 February 1992)

A direct comparison is made between the dynamics obtained by weakly nonlinear theory and full numerical simulations for Langmuir circulations in a density-stratified layer having finite depth and infinite horizontal extent. In one limit, the mathematical formulation employed is analogous to that of double-diffusion phenonema with the flux of one diffusing quantity fixed at the boundaries of the layer. These problems have multiple bifurcation points, but their amplitude equations have no intrinsic (nonlinear) degeneracies, in contrast to 'standard' double-diffusion problems. The symmetry of the physical problem implies invariance with respect to translations and reflections in the horizontal direction normal to the applied wind stress (so-called $O(2)$ symmetry). A multiple bifurcation at a double-zero point serves as an organizing centre for dynamics over a wide range of parameter values. This double zero, or Takens–Bogdanov, bifurcation leads to doubly periodic motions manifested as modulated travelling waves. Other multiple bifurcation points appear as double-Hopf bifurcations. It is believed that this paper gives the first quantitative comparison of dynamics of double-diffusive type predicted by rationally derived amplitude equations and by full nonlinear partial differential equations. The implications for physically observable natural phenomena are discussed. This problem has been treated previously, but the earlier numerical treatment is in error, and is corrected here. When the Stokes drift gradient due to surface waves is not constant, the analogy with the common formulations of double-diffusion problems is compromised. Our bifurcation analyses are extended here to include the case of exponentially decaying Stokes drift gradient.

1. Introduction

The mechanically driven convective motions in the upper layers of the ocean and other natural bodies of water, known as Langmuir circulations (LC) characteristically take the form of rolls with axes nearly parallel to the direction of the applied wind stress. In the theory of Craik & Leibovich (1976) – see Leibovich (1983) for a survey of the phenomenon and the subsequent development of this theoretical framework – Langmuir circulations are mathematically analogous to other more familiar convective processes in certain limits. In particular, when spatial variation in the wind direction is neglected, the motion takes place in a layer of finite depth, and the

† Present address: Department of Applied Mathematics, The University of Adelaide, G.P.O. Box 498, Adelaide 5001, South Australia.

Stokes drift gradient associated with surface waves is approximated as constant, then direct mathematical analogies are possible. When the water has uniform density, the analogy is to Bénard convection, and when the water is density stratified, the analogy is to thermohaline (or double-diffusive) convection. When this analogy is invoked, not all of the boundary conditions appropriate to a buoyancy-driven flow are relevant to the LC problem, but those relevant to LC are contained in those that may sensibly be imposed to model buoyancy-driven flows.

These analogies have been explored by Moroz & Leibovich (1985) and especially by Leibovich, Lele & Moroz (1989, hereinafter referred to as LLM), based on a model introduced by Leibovich (1985) for Langmuir circulations in a stratified layer bounded below by a strong thermocline. In this model, the stress transmitted across the layer is constant, and the temperature (the only agency considered to cause stratification) is held fixed at the top and bottom of the layer. This is analogous to a double-diffusion problem with fixed flux at the boundaries for one diffusing quantity, and fixed level for the second diffusing quantity. LLM present linear stability results, and address the nonlinear dynamics, which are shown to lead to various transition sequences which are decisively different depending on whether the sidewall boundary conditions are chosen to be periodic or flux-free. The direct numerical simulations done in LLM are in error, however, and these are corrected in Appendix A to the present paper. The new results differ quantitatively and qualitatively for both periodic and flux-free conditions. Given the disputed nature of the numerical work, we have gone to considerable pains, detailed in Appendix B, to verify the correctness of the numerical procedures used here.

We also give additional results for exponentially decaying Stokes drift, a problem not directly analogous to double diffusion.

Our main focus in this paper is the comparison between dynamical behaviour predicted by the weakly nonlinear theory and the full partial differential equations when periodic lateral boundary conditions are imposed. To this end, we derive amplitude equations that describe the nonlinear dynamics near bifurcations from the basic state. The physical problem posed has $O(2)$ symmetry, that is, the problem is invariant with respect to arbitrary translations in the crosswind horizontal direction, and to reflections of this direction. Such symmetry is common, and leads to multiple eigenvalues in the linear stability problem; furthermore, multiple bifurcation points can arise, especially when the problem has two independent control parameters. This is the case here, with the effect of wind and surface wave forcing represented by a destabilizing 'Rayleigh' number, R, and the buoyancy represented by a stabilizing Rayleigh number, S: these characterizations assume, as we do throughout, that attention is restricted to the first (S, R)-quadrant.

The nonlinear dynamics depend on the specification of the horizontal spatial period under consideration. In the body of the paper, this is fixed to be twice the depth of the layer. The dynamical behaviour near the instability onset depends on S. In the case of constant Stokes-drift gradient, stability is first lost to steady states when $S < S^{\mathrm{D}} \approx 72.01$, while for $S > S^{\mathrm{D}}$ stability is first lost to oscillatory convection.

The physical consequence of the $O(2)$ symmetry is to allow stable travelling waves and stable modulated travelling waves. Both possibilities are captured by analysis in the vicinity of a multiple bifurcation point associated with a double-zero eigenvalue, the so-called Takens–Bogdanov bifurcation (see Dangelmayr & Knobloch 1987 for a thorough treatment of the general dynamical possibilities). This double-zero bifurcation serves as the organizing centre, in the sense that the dynamics near this point capture the dynamical behaviour of the full system even at points at some

distance in parameter space from the multiple bifurcation. For larger values of S, a sequence of other multiple bifurcation points is encountered, each of which is a double-Hopf bifurcation (two pairs of imaginary eigenvalues). These seem not to play the central role of the double zero, which still seems to organize the dynamics. A discussion of a double-Hopf bifurcation in this system will be presented elsewhere (Cox *et al.* 1992).

Travelling waves and modulated travelling waves, as well as other possibilities, have been predicted on the basis of amplitude equations (including those for the Takens–Bogdanov bifurcation) and full numerical simulations of two-dimensional double diffusion with 'standard' choices for boundary conditions (both diffusing substances constant on the horizontal boundaries). In these problems, which, like LLM, we will refer to as 'ideal double diffusion' (IDD), the linearized problem can be solved in closed form, and the cubic terms in the amplitude equations can be computed analytically. The bifurcation in these cases has a (nonlinear) degeneracy marked by the vanishing of the coefficient in one of the cubic terms that determines the stability of travelling waves. As a consequence, the dynamics are not fully specified to third order, and matters are not settled until quintic terms are included. In this case, Knobloch (1985) finds that standing waves are never stable near bifurcation. While the range of possible qualitative dynamics allowed by the amplitude equations can be determined and is found to include cases computed from the partial differential equations (see Deane, Knobloch & Toomre 1987 and Knobloch, Deane & Toomre 1987, for ideal double diffusion, and Knobloch & Moore 1990*a*, *b* for binary fluid convection), a detailed comparison of dynamics has not been made, to our knowledge, for any previously studied problem with $O(2)$ symmetry that admits stable, self-excited, travelling waves.

By contrast, the weakly nonlinear theory of the problem addressed here is determined by the cubic nonlinearities for sufficiently small amplitude. Numerical computation is required to compute the coefficients in the amplitude equations in this case. We do this, and are able to make definitive comparisons between the predictions of weakly nonlinear theory and full simulations.

The problem formulation and the linearized theory are outlined in §2, followed in §3 by the analysis needed to derive the weakly nonlinear problem for steady convection, oscillatory convection (the simple Hopf bifurcation with $O(2)$ symmetry), and the double-zero bifurcation in which steady and oscillatory convection patterns may compete. The dynamical behaviour encompassed by the amplitude equations is described in §4. Direct numerical simulations of the partial differential equations are described in §5 and compared to the bifurcation analyses for periodic boundary conditions. A brief discussion of the spatial symmetries satisfied by the various solutions (steady states, travelling waves, and standing waves) is given in §6, and conclusions are given in §7. Simulations with both flux-free and periodic boundary conditions are described in Appendix A, which together with §5 provides detailed corrections to the simulations given by LLM. Appendix B describes the pseudo-spectral code used for the numerical simulations. Appendix C describes how the computer algebra methods we use for the bifurcation analyses are implemented. The latter are based on the methods introduced by Mahalov & Leibovich (1991*a*, *b*).

2. Problem formulation and linearized stability

2.1. *Problem statement*

A horizontally infinite layer of stratified water is bounded by a free surface with mean location at $z = 0$, and a lower bounding plane at $z = -d$. The free surface supports water waves with time-independent, horizontally homogeneous characteristics. The water waves are associated with a Stokes drift u_s, and we write the gradient of the drift as

$$\frac{\partial u_s}{\partial z} = \frac{\partial u_s}{\partial z}(0)\, h(z/d),$$

where h is a dimensionless function. After averaging as in Craik & Leibovich (1976), and Leibovich (1977*a*, *b*), the surface waves are filtered out, and the plane at $z = 0$ serves as the upper boundary for the purposes of our analysis. The wind exerts a constant stress, ρu_*^2, in the x-direction, and the water temperature is held constant at the upper and lower boundaries of the layer. The lower boundary is thought of as marking a strong thermocline inhibiting vertical motions and separating the layer of interest from a deep body of water below. Following LLM, we assume that the stress transmitted to the water below is also constant in time and equal to that imparted to the upper surface.

An equilibrium flow consisting of a linear shear

$$U(z) = (u_*^2/\nu_T)\, z + U_0,$$

and a linear temperature profile

$$T(z) = (\Delta T/d)\, z + T(0),$$

is admissible, where ν_T is the eddy viscosity, and ΔT is the difference between the temperature at the lower and upper boundaries (assumed positive here).

We are interested in Langmuir circulations in this layer arising as perturbations to the equilibrium, with spatial variations in the x-direction ignored. The reader is referred to §2 of LLM for a discussion of the mathematical description that we shall adopt. The present model does not produce a finite critical wavenumber, and so we must decide (somewhat arbitrarily) on an aspect ratio for the motions. A more general mathematical model of a stratified water layer bounded below by a strong thermocline given in Cox & Leibovich (1992) does yield a finite horizontal lengthscale for the motions and thereby avoids the need for an arbitrary quantization, but this model will not be considered here.

With d as scale for length, d^2/ν_T as scale for time, ν_T/d as scale for the perturbation velocity in the crosswind (y,z)-plane, and $\Delta U \equiv U(0) - U(-d)$ as scale for the perturbation velocity component in the x-direction, the dimensionless wave-filtered equations of motion are

$$\left(\frac{\partial}{\partial t} - \nabla^2\right)\nabla^2\psi = Rh(z)\frac{\partial u}{\partial y} - S\frac{\partial \theta}{\partial y} + \mathbf{J}(\psi, \nabla^2\psi), \tag{1}$$

$$\left(\frac{\partial}{\partial t} - \nabla^2\right)u = \frac{\partial \psi}{\partial y} + \mathbf{J}(\psi, u), \tag{2}$$

$$\left(\frac{\partial}{\partial t} - \tau\nabla^2\right)\theta = \frac{\partial \psi}{\partial y} + \mathbf{J}(\psi, \theta), \tag{3}$$

where u is the perturbation velocity component in the x-direction, θ is the perturbation temperature, and ψ is the stream function in the crossplane. Here the dimensionless (y, z) velocity components (v, w) are given by

$$v = \frac{\partial \psi}{\partial z}, \quad w = -\frac{\partial \psi}{\partial y},$$

and $\mathbf{J}(f, g)$ is the Jacobian

$$\mathbf{J}(f, g) = \frac{\partial f}{\partial y}\frac{\partial g}{\partial z} - \frac{\partial f}{\partial z}\frac{\partial g}{\partial y}.$$

The 'Rayleigh number' parameters, R and S, and the parameter τ are given by

$$R = \frac{\Delta U d^3}{\nu_T^2}\frac{\partial u_s}{\partial z}(0), \quad S = \frac{\beta g \Delta T d^3}{\nu_T^2}, \quad \tau = \frac{\alpha_T}{\nu_T},$$

where β is the coefficient of volume expansion, g the gravitational acceleration, and α_T the eddy diffusivity of heat.

The dimensionless Stokes drift gradient may be taken to be any appropriate function of depth; here it is taken here to be a simple exponential

$$h(z) = \exp(2\lambda z), \tag{4}$$

which is appropriate to a monochromatic surface wave train. The analogy with two-dimensional thermohaline convection with Prandtl number unity holds when $\lambda = 0$, and is then obtained by identifying R and S as the thermal and salt Rayleigh numbers, and τ the ratio of salt to heat diffusivities. If Θ and Σ are the temperature and salt perturbations, then the analogy identifies $u \mapsto -\Theta$ and $\theta \mapsto -\Sigma$.

Since the stress and temperature at the bounding horizontal surfaces are held constant, the perturbations to these quantities vanish there, together with the normal velocity component, so

$$\frac{\partial u}{\partial z} = \frac{\partial^2 \psi}{\partial z^2} = y = v = 0 \quad \text{at} \quad z = 0, -1. \tag{5}$$

In LLM, two types of lateral boundary conditions were considered: periodic with period L, appropriate when $O(2)$ symmetry is considered, and 'constrained'. The 'constrained' boundary condition is periodic, but forces fluxes to vanish at the lateral boundaries, or

$$\psi = \frac{\partial^2 \psi}{\partial y^2} = \frac{\partial u}{\partial y} = \frac{\partial \theta}{\partial y} = 0 \quad \text{at} \quad y = 0, L. \tag{6}$$

We refer to such boundary conditions as 'flux-free'.

The LC problem may be written in abstract form as

$$\mathbf{L}\Psi = \mathbf{N}(\Psi, \Psi), \tag{7}$$

subject to the boundary conditions

$$\mathbf{B}\Psi = \mathbf{0}, \tag{8}$$

where $\Psi = (\psi, u, \theta)$ is the perturbation to the basic state, $\mathbf{L}$ is the linear operator, $\mathbf{N}$ the (nonlinear) Jacobian, and $\mathbf{B}$ the (linear) boundary condition operator.

2.2. *Summary of relevant linear stability results*

Linear stability is determined by

$$\mathbf{L}\Psi = \mathbf{0}. \tag{9}$$

The linear operator $\mathbf{L}$ may be written as

$$\mathbf{L} = \partial_t \mathbf{J} + \mathbf{K},$$

where the operators $\mathbf{J}$ and $\mathbf{K}$ involve ∂_y and ∂_z, but not ∂_t. The operator $\mathbf{J}$ is the self-adjoint diagonal matrix operator

$$\mathrm{diag}\,[\nabla^2, 1, 1],$$

and the operator $\mathbf{K}$ is the matrix operator

$$\mathbf{K} = -\begin{pmatrix} \nabla^4 & R_c \dfrac{\partial}{\partial y} & -S\dfrac{\partial}{\partial y} \\ \dfrac{\partial}{\partial y} & \nabla^2 & 0 \\ \dfrac{\partial}{\partial y} & 0 & \tau\nabla^2 \end{pmatrix}. \tag{10}$$

Here R_c is the critical value of R, given S, L, λ and τ, for onset of convective motion from the non-convective equilibrium.

The formal construction of weakly nonlinear amplitude equations requires the solution of the adjoint linear problem. The linear problem (9) is not self-adjoint, since $\mathbf{K}$ is not: nevertheless, we can determine the adjoint eigenfunctions $\Psi^\dagger$ from the eigenfunctions of (9) in the important special case $\lambda = 0$. The relation is

$$\Psi^\dagger = \begin{pmatrix} 1 & 0 & 0 \\ 0 & -R_c & 0 \\ 0 & 0 & S \end{pmatrix} \Psi^*,$$

where $(\,)^*$ indicates complex conjugation.

We determine the linear stability of the basic state by the method of normal modes, that is, we consider disturbances of the form

$$\Psi = \hat{\Psi}(z)\, e^{iky+\sigma t} = (\hat{\psi}(z), \hat{u}(z), \hat{\theta}(z))\, e^{iky+\sigma t},$$

where

$$k = 2\pi/L,$$

and find the growth rate, σ, by solving the eigenvalue problem

$$\{\sigma \mathbf{J}(k) + \mathbf{K}(k)\}\,\hat{\Psi} = \mathbf{0}. \tag{11}$$

Here, the operators $\mathbf{J}(k)$ and $\mathbf{K}(k)$ are obtained from $\mathbf{J}$ and $\mathbf{K}$ by replacing ∂_y by ik. Thus they depend upon ∂_z, but not upon ∂_y or ∂_t. The eigenvalue, σ_1, with the largest real part determines the stability of the basic state. If $\mathrm{Re}\,(\sigma_1) > 0$ then the basic state is unstable. Stability is lost as the Rayleigh number increases through the critical value, R_c; to steady convection if $\mathrm{Im}\,(\sigma_1) = 0$, and to oscillatory convection otherwise, if $\sigma_1 = i\omega \neq 0$. We regard the parameters λ and τ as fixed, and we increase R for fixed S, or vary both R and S independently.

Numerical simulation of the nonlinear problem requires a choice of the lateral dimensions of the computational region. LLM considered motions with fundamental periods of both $L = 2$ (i.e. $k = \pi$) and $L = 4 (k = \frac{1}{2}\pi)$; see their paper for a justification. Except for Appendix A, where both fundamental periods are treated, we focus attention on $L = 2$. With this fundamental, the marginal linear stability boundary

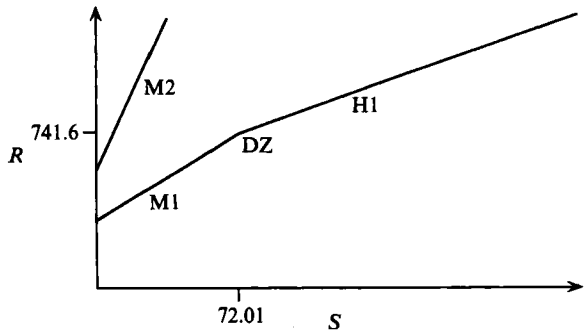

FIGURE 1. Stability diagram for $L = 2$. 'M1' indicates transition to a monotonic convective state, 'H1' a Hopf bifurcation to oscillatory convection, for the fundamental mode with horizontal wavenumber π. The intersection at $(S^{\mathrm{D}}, R^{\mathrm{D}}) \approx (72.01, 741.6)$ is a double-zero (DZ) bifurcation. 'M2' indicates the monotonic bifurcation of the mode with wavenumber 2π.

for the nonconvective state in the (S, R)-plane is sketched in figure 1. The boundary consists of a series of intersecting curves (this is seen more clearly in figure 12), each almost a straight line. For $S < S^{\mathrm{D}}$, stability is first lost (on linear grounds), as R increases, to a steady convective motion, while for $S > S^{\mathrm{D}}$, stability is first lost to oscillatory motion. LLM quote an approximate value for S^{D} of 78: we have determined that a more accurate value is 72.01.

3. Weakly nonlinear analysis

Near a bifurcation point $(R_{\mathrm{c}}, S_{\mathrm{c}})$ we can write the solution $\boldsymbol{\Psi}$ as a power series in the small parameter ϵ, where $\epsilon = O(|(R, S) - (R_{\mathrm{c}}, S_{\mathrm{c}})|^{\frac{1}{2}})$. If a single eigenmode becomes unstable at $(R_{\mathrm{c}}, S_{\mathrm{c}})$ then to leading order in ϵ, $\boldsymbol{\Psi}$ is proportional to the marginal eigenfunction, with an amplitude that evolves according to an 'amplitude equation', an ordinary differential equation that can be rationally derived from the full nonlinear system. If two or more modes simultaneously destabilize then $\boldsymbol{\Psi}$ is approximately a sum of these modes, with the amplitude of each mode evolving according to an amplitude equation. In this problem, there are four cases to consider.

In the first and simplest case, a single eigenvalue of the linear operator $\mathbf{L}$ passes through zero as R is increased through R_{c}; this occurs when $S < S^{\mathrm{D}}$. The derivation of the Landau equation from the full partial differential equations in this case is standard.

In the second case, which arises when $S = S^{\mathrm{D}}$, the operator $\mathbf{L}$ has a double-zero eigenvalue at onset. The derivation of the (system of) Landau equations from the full partial differential equations is somewhat more complicated. The procedures are not yet standard and we give a full account. The resulting pair of complex amplitude equations turns out to describe the dynamics of the fully nonlinear problem over a wide range of parameter values. In this sense, the double-zero bifurcation point serves as an 'organizing centre' for an important range of the nonlinear dynamics.

In the third case, a pair of complex-conjugate eigenvalues crosses the real axis as R increases through its critical value, thus leading to a Hopf bifurcation. Again, because of the $O(2)$ symmetry, a pair of complex amplitude equations is required to describe this bifurcation. This third case occurs for all $S > S^{\mathrm{D}}$, except at isolated points.

These exceptional points are the intersections at which *two* spatial modes, each associated with a pair of imaginary eigenvalues, coexist on the marginal stability

boundary. These form the fourth case, and lead to double-Hopf bifurcations. In the presence of $O(2)$ symmetry, systems of four complex amplitude equations are required to complete the description of the local dynamics near these points.

We outline the results of all four of these cases below, but give a detailed description of the derivation of amplitude equations only in the first two. For a full account of the details of the bifurcation analyses (both Hopf and double Hopf) to oscillatory convection see Cox *et al.* (1992), where both the $O(2)$-symmetric periodic problem and the Z_2-symmetric flux-free problem are treated.

3.1. *A single zero eigenvalue (steady bifurcation)*

We consider first the case where $\sigma_1 = 0$ at the bifurcation point, and expand $\boldsymbol{\Psi}$ as a power series in ϵ,

$$\boldsymbol{\Psi} = \epsilon \boldsymbol{\Psi}_1 + \epsilon^2 \boldsymbol{\Psi}_2 + \epsilon^3 \boldsymbol{\Psi}_3 + \dots. \tag{12}$$

Linear theory tells us that the growth rate of the convection cells is

$$O(|R-R_c, S-S_c)|),$$

and a possible nonlinear balance is indicated when $|(R-R_c, S-S_c)| = O(\epsilon^2)$. We therefore take $R = R_c + \epsilon^2 R_2$, $S = S_c + \epsilon^2 S_2$, and introduce a slow timescale $T = \epsilon^2 t$ for the evolution of the amplitude of convection. Specifically, we write

$$\frac{\partial}{\partial t} \mapsto \frac{\partial}{\partial t} + \epsilon^2 \frac{\partial}{\partial T}.$$

Since $\mathbf{K}(k)$ depends on R and S then we must expand this operator also,

$$\mathbf{K}(k) = \mathbf{K}_0(k) + \epsilon^2 R_2 \mathbf{K}_R(k) + \epsilon^2 S_2 \mathbf{K}_S(k) + O(\epsilon^4),$$

where $\mathbf{K}_R = \partial \mathbf{K}(k)/\partial R$ and $\mathbf{K}_S = \partial \mathbf{K}(k)/\partial S$. In a standard way, but using a computer algebra package to carry out the details, we solve the problems that result from considering the terms in the governing equations at successive powers in ϵ. The practical details of carrying this out numerically are described in Appendix C.

The problem at $O(\epsilon)$ is just the eigenvalue problem,

$$\mathbf{K}_0(k)\, \hat{\boldsymbol{\Psi}}_0(z) = \mathbf{0}, \tag{13}$$

where the leading term for $\boldsymbol{\Psi}$ is

$$\boldsymbol{\Psi}_1 = A(T)\, \hat{\boldsymbol{\Psi}}_0(z)\, \mathrm{e}^{\mathrm{i}ky} + \text{c.c.};$$

$A(T)$ is the slowly varying amplitude and c.c. in this and in subsequent expressions stands for the complex conjugate of the preceding term. We normalize the eigenfunction $\hat{\boldsymbol{\Psi}}_0(z)$ so that

$$\int_{-1}^{0} |\hat{\psi}(z)|^2 \, \mathrm{d}z = \tfrac{1}{2}.$$

With this choice, when we change the boundary conditions to check our calculations against ideal double diffusion, we can make a direct comparison of the coefficients of the nonlinear terms since for that problem, $\hat{\psi}(z) = \sin \pi z$, which satisfies our normalization.

At $O(\epsilon^2)$ we have

$$\mathbf{K}_0\, \boldsymbol{\Psi}_2 = \mathbf{N}(\boldsymbol{\Psi}_1, \boldsymbol{\Psi}_1).$$

The right-hand side of this equation consists of terms proportional to

$$A^2 \mathrm{e}^{2\mathrm{i}ky}, \; A^{*2} \mathrm{e}^{-2\mathrm{i}ky} \text{ and } |A|^2.$$

We denote these terms by $\boldsymbol{R}_2^{(2)}$, $\boldsymbol{R}_2^{(-2)}$ and $\boldsymbol{R}_2^{(0)}$, respectively. To solve for the corresponding components of $\boldsymbol{\Psi}_2$ we have

$$\mathbf{K}_0(\pm 2k)\,\boldsymbol{\Psi}_2^{(\pm 2)} = \boldsymbol{R}_2^{(\pm 2)} \tag{14}$$

$$\mathbf{K}_0(0)\,\boldsymbol{\Psi}_2^{(0)} = \boldsymbol{R}_2^{(0)}, \tag{15}$$

where $$\boldsymbol{\Psi}_2 = \boldsymbol{\Psi}_2^{(+2)}\,\mathrm{e}^{+2\mathrm{i}ky} + \boldsymbol{\Psi}_2^{(0)} + \boldsymbol{\Psi}_2^{(-2)}\,\mathrm{e}^{-2\mathrm{i}ky}.$$

Since the solution is real, $\boldsymbol{\Psi}_2^{(-2)} = \boldsymbol{\Psi}_2^{(+2)*}$, and we need calculate only one of $\boldsymbol{\Psi}_2^{(-2)}$ and $\boldsymbol{\Psi}_2^{(+2)}$. We assume, as is generally the case, that neither $\mathbf{K}_0(2k)$ nor $\mathbf{K}_0(0)$ has a zero eigenvalue, that is, that there are no resonances in our choice of parameters.

To find $\boldsymbol{\Psi}_3$ we need to solve

$$\mathbf{K}_0\,\boldsymbol{\Psi}_3 = \mathbf{N}(\boldsymbol{\Psi}_1, \boldsymbol{\Psi}_2) + \mathbf{N}(\boldsymbol{\Psi}_2, \boldsymbol{\Psi}_1) - \left\{\left[(R_2\,\mathbf{K}_R(k) + S_2\,\mathbf{K}_S(k))\,A(T)\,\hat{\boldsymbol{\Psi}}_0(z) + \mathbf{J}(k)\frac{\mathrm{d}A}{\mathrm{d}T}\,\hat{\boldsymbol{\Psi}}_0(z)\right] + \text{c.c.}\right\}. \tag{16}$$

The right-hand side of this equation contains terms proportional to $\mathrm{e}^{\pm 3\mathrm{i}ky}$ and $\mathrm{e}^{\pm \mathrm{i}ky}$. The latter terms impose a secular forcing, and in order to ensure the validity of the expansion (12), we choose $\mathrm{d}A/\mathrm{d}T$ so as to remove this secular term, ensuring that the right-hand side lies in the range of $\mathbf{K}_0(k)$. This gives us the Landau equation governing the evolution of A. We need consider only $\boldsymbol{\Psi}_3^{(+1)}$, the component of $\boldsymbol{\Psi}_3$ proportional to $\mathrm{e}^{\mathrm{i}ky}$, and $\boldsymbol{R}_3^{(1)}$, the part of the right-hand side proportional to $\mathrm{e}^{\mathrm{i}ky}$.

The terms in (16) proportional to $\mathrm{e}^{\mathrm{i}ky}$ are

$$\mathbf{K}_0(k)\,\boldsymbol{\Psi}_3^{(1)} = \mathbf{N}^{(1)} - (R_2\,\mathbf{K}_R(k) + S_2\,\mathbf{K}_S(k))\,A(T)\,\hat{\boldsymbol{\Psi}}_0(z) - \mathbf{J}(k)\frac{\mathrm{d}A}{\mathrm{d}T}\,\hat{\boldsymbol{\Psi}}_0(z), \tag{17}$$

where $\mathbf{N}^{(1)}$ represents all the nonlinear terms of order ϵ^3 proportional to $\mathrm{e}^{\mathrm{i}ky}$, and is proportional to $A|A|^2$. Formally, in order to find the amplitude equation for A we take the inner product of (17) with the linear adjoint solution, $\boldsymbol{\Psi}^\dagger$. This gives

$$\langle \boldsymbol{\Psi}^\dagger, \mathbf{J}(k)\,\hat{\boldsymbol{\Psi}}_0\rangle \frac{\mathrm{d}A}{\mathrm{d}T} = A(T)\{-\langle \boldsymbol{\Psi}^\dagger, \mathbf{K}_R\,\hat{\boldsymbol{\Psi}}_0\rangle R_2 - \langle \boldsymbol{\Psi}^\dagger, \mathbf{K}_S\,\hat{\boldsymbol{\Psi}}_0\rangle S_2\} + \langle \boldsymbol{\Psi}^\dagger, \mathbf{N}^{(1)}\rangle, \tag{18}$$

and so the amplitude equation

$$\dot{A} \equiv \frac{\mathrm{d}A}{\mathrm{d}T} = A\{\mu + \alpha|A|^2\}. \tag{19}$$

Here, μ is a linear combination of R_2 and S_2. If $\alpha > 0$ then the bifurcation to steady convection is subcritical, while if $\alpha < 0$ the bifurcation is supercritical. In the practical implementation used in our numerical work, the coefficients in (19) are evaluated by a method that does not require explicit calculation of inner products with the adjoint. This will be described in Appendix C.

3.2. *A pair of imaginary eigenvalues (Hopf bifurcation)*

When $\mathrm{Im}\,(\sigma_1) = \mathrm{i}\omega \neq 0$ at the bifurcation point then nearby in parameter space there are time-periodic solutions with period near that of linear theory, that is, $|2\pi/\omega|$. The $O(2)$ symmetry is manifested by the fact (see Knobloch 1985) that $\pm\mathrm{i}\omega$, ω real, are both eigenvalues for the same wavenumber, k. There are consequently two possible linear modes, one corresponding to a travelling wave (TW) moving to the right (positive y-direction), and a second one corresponding to a TW moving to the left.

In addition, any linear combination of these TW is possible on linear grounds. The potentially significant one of these is the standing wave (SW), which is the combination of the two TW having equal amplitudes.

The linear solution, $\boldsymbol{\Psi}_1$, takes the form

$$\boldsymbol{\Psi}_1 = \{A_1(T)\,\mathrm{e}^{\mathrm{i}ky+\mathrm{i}\omega t}\,\boldsymbol{\Psi}_{11}(z) + A_2(T)\,\mathrm{e}^{\mathrm{i}ky-\mathrm{i}\omega t}\,\boldsymbol{\Psi}_{12}(z)\} + \text{c.c.}, \tag{20}$$

where $\boldsymbol{\Psi}_{11} = \hat{\boldsymbol{\Psi}}_0(z) = (\hat{\psi}_0, \hat{u}_0, \hat{\theta}_0)$ and $\boldsymbol{\Psi}_{12} = (-\hat{\psi}_0^*, \hat{u}_0^*, \hat{\theta}_0^*)$. Clearly A_1 is the amplitude of the left-TW, and A_2 and the amplitude of the right-TW.

The amplitude equations for A_1 and A_2 are

$$\dot{A}_1 = A_1\{\mu + \alpha|A_1|^2 + \beta|A_2|^2\}, \tag{21}$$

$$\dot{A}_2 = A_2\{\mu^* + \beta^*|A_1|^2 + \alpha^*|A_2|^2\}. \tag{22}$$

There are four possible steady states, which correspond to the rest state, to left- and right-TW, and to an SW.

The stability of these four states is easily analysed. One finds (see Knobloch 1985) that TW and SW are unstable unless both bifurcate supercritically (so $\alpha_\mathrm{r} < 0$ and $\alpha_\mathrm{r} + \beta_\mathrm{r} < 0$, where the subscript r denotes the real part). In that case, the one with the larger amplitude is stable and the other is unstable.

3.3. *A pair of zero eigenvalues (Takens–Bogdanov bifurcation)*

Our linear stability analysis indicates that at the codimension point

$$(R, S) = (R^\mathrm{D}, S^\mathrm{D}) \approx (741.64, 72.01)$$

the linear operator $\mathbf{L}$ has a pair of zero eigenvalues for modes with wavenumber $k = \pi$. This is the so-called $O(2)$-symmetric Takens–Bogdanov bifurcation, in the neighbourhood of which several dynamical scenarios are possible (Knobloch 1986; Dangelmayr & Knobloch 1986, 1987). New types of solutions are possible near the coalescence of the steady and Hopf bifurcations, which are not predicted by an investigation of each of the simpler bifurcations independently. For example, two-frequency motions, representing modulated travelling waves, are possible.

At the codimension-two point, $\mathbf{L}$ has a deficient zero-eigenspace: there is one genuine eigenfunction, and one generalized eigenfunction. A linear analysis indicates that disturbances proportional to the zero eigenmode grow like t, while disturbances proportional to the generalized eigenmode neither grow nor decay. A consequence of this secular growth of the linearized disturbances is that we must abandon the straightforward two-timescale expansion that we have previously used near the single steady and Hopf bifurcations. A modified two-time procedure can be used, but we prefer to proceed by expanding quantities in powers of the amplitudes of the genuine and the generalized zero-eigenmodes (as in, for example, Rubenfeld 1978, who discusses the process for ordinary differential equations), but we make no assumption about the timescales of the motion. We write

$$\boldsymbol{\Psi} \equiv (\psi, u, \theta) = \{A_1(t)\,\hat{\boldsymbol{\Psi}}_1(z)\,\mathrm{e}^{\mathrm{i}ky} + A_2(t)\,\hat{\boldsymbol{\Psi}}_2(z)\,\mathrm{e}^{\mathrm{i}ky}\} + \text{c.c.} + O(|(A_1, A_2)|^2), \tag{23}$$

where $(R,S)-(R^\mathrm{D},S^\mathrm{D}) = O(|(A_1,A_2)|^2)$. The evolution of the amplitudes may be described by the normal form

$$\left.\begin{aligned} \mathrm{d}A_1/\mathrm{d}t &= A_2, \\ \mathrm{d}A_2/\mathrm{d}t &= \mu A_1 + \nu A_2 + [a|A_1|^2 + b|A_2|^2 + c(A_1 A_2^* + A_1^* A_2)]A_1 + d|A_1|^2 A_2. \end{aligned}\right\} \tag{24}$$

Here, μ and ν are linear combinations of $R-R^\mathrm{D}$ and $S-S^\mathrm{D}$, and so are of order $|(A_1, A_2)|^2$. The coefficients in these equations are real, but the amplitudes are in general complex.

In order to calculate the coefficients in (24) we first expand $\boldsymbol{\Psi}$ in powers of the amplitudes A_1, A_2, so that $\boldsymbol{\Psi} = \boldsymbol{\Psi}^{(1)} + \boldsymbol{\Psi}^{(2)} + \ldots$, where $\boldsymbol{\Psi}^{(n)} = O(|(A_1, A_2)|^n)$ as $|(A_1, A_2)| \to 0$. Then we replace the operator $\partial/\partial t$ by the operator

$$\dot{A}_1 \partial/\partial A_1 + \dot{A}_2 \partial/\partial A_2,$$

where $\dot{A}_1$ and $\dot{A}_2$ are given by (24). Finally we solve the equations that arise at successive powers of the amplitudes in the governing equations. As for the previous analysis of the steady and Hopf bifurcations, in practice we represent functions of z by truncated sums of Chebyshev polynomials, thereby transforming the ordinary differential problems into algebraic ones, and functions of z into vectors of coefficients of Chebyshev polynomials, as described in Appendix C.

At leading order, the following equations must be solved for $\hat{\boldsymbol{\Psi}}_1(z)$ and $\hat{\boldsymbol{\Psi}}_2(z)$:

$$\left.\begin{aligned} \text{at } O(A_1): \quad & \mathbf{K}_0(k)\,\hat{\boldsymbol{\Psi}}_1(z) = \mathbf{0}, \\ \text{at } O(A_2): \quad & \mathbf{J}(k)\,\hat{\boldsymbol{\Psi}}_1 + \mathbf{K}_0(k)\,\hat{\boldsymbol{\Psi}}_2(z) = \mathbf{0}. \end{aligned}\right\} \tag{25}$$

Evidently, $\hat{\boldsymbol{\Psi}}_1(z)$ is an eigenfunction of the operator $\mathbf{J}^{-1}(k)\,\mathbf{K}_0(k)$ corresponding to a zero eigenvalue, and $\hat{\boldsymbol{\Psi}}_2(z)$ is a generalized eigenfunction of $\mathbf{J}^{-1}(k)\,\mathbf{K}_0(k)$.

At $O(|A_1, A_2)|^2)$, $\boldsymbol{\Psi}^{(2)}$ is of the form

$$\begin{aligned} \boldsymbol{\Psi}^{(2)} = {} & A_1^2\,\hat{\boldsymbol{\Psi}}_3\,\mathrm{e}^{2iky} + [A_1^{*2}\,\boldsymbol{\Psi}_3^*\,\mathrm{e}^{-2iky}] + |A_1|^2\,\hat{\boldsymbol{\Psi}}_4 + \mathbf{A}_1\mathbf{A}_2\,\hat{\boldsymbol{\Psi}}_5\,\mathrm{e}^{2iky} + [A_1^* A_2^*\,\boldsymbol{\Psi}_5^*\,\mathrm{e}^{-2iky}] \\ & + A_1^* A_2\,\hat{\boldsymbol{\Psi}}_6 + A_1 A_2^*\,\hat{\boldsymbol{\Psi}}_6^* + A_2^2\,\hat{\boldsymbol{\Psi}}_7\,\mathrm{e}^{2iky} + [A_2^{*2}\,\hat{\boldsymbol{\Psi}}_7^*\,\mathrm{e}^{-2iky}] + |A_2|^2\,\hat{\boldsymbol{\Psi}}_8, \end{aligned} \tag{26}$$

where we do not need to account explicitly for the terms in square brackets because they do not contribute to the coefficients in the evolution equations for A_1 and A_2 to the order we will consider. The components $\hat{\boldsymbol{\Psi}}_i(z)$ may be found sequentially from the linear inhomogeneous equations that arise at appropriate powers in the amplitude expansion of the governing equation.

A practical consequence of the coupling of A_1 and A_2 is that the operator $\partial/\partial t$ no longer splits into a constant frequency of oscillation plus a much slower modulation, but now contains a non-trivial contribution of $O(1)$, $\dot{A}_2 \partial/\partial A_1$. At each order in $|(A_1, A_2)|$, therefore, we are not free to solve for the terms proportional to $A_1^{i_1} A_2^{i_2} A_1^{*i_3} A_2^{*i_4}$ in any order as we are for the single bifurcations. At $O(|A_1, A_2)|^m)$, say, we must first compute the terms with $i_1 + i_3 = m$, then the terms with $i_1 + i_3 = m - 1$, and so on. This is exemplified at first order by our having to solve first the equation at $O(A_1)$, then that at $O(A_2)$ in (25). At second order, we must solve first for $\hat{\boldsymbol{\Psi}}_3$ and $\hat{\boldsymbol{\Psi}}_4$. These components satisfy the following equations:

$$\mathbf{K}_0(2k)\,\hat{\boldsymbol{\Psi}}_3 = \mathbf{N}(A_1^2), \tag{27}$$

$$\mathbf{K}_0(0)\,\hat{\boldsymbol{\Psi}}_4 = \mathbf{N}(|A_1|^2), \tag{28}$$

where $\mathbf{N}(A_1^2)\mathrm{e}^{2iky}$ denotes the term proportional to $A_1^2\mathrm{e}^{2iky}$ that arises from substituting the amplitude expansion for $\boldsymbol{\Psi}$ into $\mathbf{N}(\boldsymbol{\Psi}, \boldsymbol{\Psi})$, and so on. Since in general there are no low-order resonances (so that the operators $\mathbf{K}_0(2k)$ and $\mathbf{K}_0(0)$ are invertible) then we can find $\hat{\boldsymbol{\Psi}}_3(z)$ and $\hat{\boldsymbol{\Psi}}_4(z)$ uniquely. To this order in the calculation, $\partial/\partial t = \dot{A}_2 \partial/\partial A_1$, and so the equations for the remaining second-order unknowns are

$$2\mathbf{J}(2k)\,\hat{\boldsymbol{\Psi}}_3 + \mathbf{K}_0(2k)\,\hat{\boldsymbol{\Psi}}_5 = \mathbf{N}(A_1 A_2), \tag{29}$$

$$\mathbf{J}(0)\,\hat{\boldsymbol{\Psi}}_4 + \mathbf{K}_0(0)\,\hat{\boldsymbol{\Psi}}_6 = \mathbf{N}(A_1^* A_2), \tag{30}$$

$$\mathbf{J}(2k)\,\hat{\boldsymbol{\Psi}}_5 + \mathbf{K}_0(2k)\,\hat{\boldsymbol{\Psi}}_7 = \mathbf{N}(A_2^2), \tag{31}$$

$$\mathbf{J}(0)\,(\hat{\boldsymbol{\Psi}}_6 + \hat{\boldsymbol{\Psi}}_6^*) + \mathbf{K}_0(0)\,\hat{\boldsymbol{\Psi}}_8 = \mathbf{N}(|A_2|^2). \tag{32}$$

Each of these may be solved in turn for $\hat{\Psi}_{5,6,7,8}(z)$, because the operators $\mathbf{K}_0(0)$ and $\mathbf{K}_0(2k)$ are invertible.

At third order we obtain the coefficients in (24) from solvability conditions when we consider linear inhomogeneous equations whose left-hand sides involve the operators $\mathbf{J}(k)$ and $\mathbf{K}_0(k)$. Considering only those terms proportional to e^{iky},

$$\Psi^{(3)} = e^{iky}\{(R_2\hat{\Psi}_9^{(R)}+S_2\hat{\Psi}_9^{(S)})A_1+(R_2\hat{\Psi}_{10}^{(R)}+S_2\hat{\Psi}_{10}^{(S)})A_2+A_1|A_1|^2\hat{\Psi}_{11}$$
$$+A_2|A_1|^2\hat{\Psi}_{12}+A_2^*A_1^2\hat{\Psi}_{13}+A_1|A_2|^2\hat{\Psi}_{14}+A_2^2A_1^*\hat{\Psi}_{15}+A_2|A_2|^2\hat{\Psi}_{16}\}, \quad (33)$$

where $(R_2,S_2)=(R-R^D,S-S^D)$. Then at $O(|A_1,A_2)|^3)$, the time derivative of the component of Ψ proportional to e^{iky} is

$$\frac{\partial\Psi}{\partial t} = e^{iky}\{(\mu A_1+\nu A_2+[a|A_1|^2+b|A_2|^2+c(A_1A_2^*+A_1^*A_2)]A_1+d|A_1|^2A_2)\hat{\Psi}_2$$
$$+(R_2\hat{\Psi}_9^{(R)}+S_2\hat{\Psi}_9^{(S)})A_2+2A_2|A_1|^2\hat{\Psi}_{11}+A_1^2A_2^*\hat{\Psi}_{11}$$
$$+A_1^*A_2^2\hat{\Psi}_{12}+A_1|A_2|^2(\hat{\Psi}_{12}+2\hat{\Psi}_{13})+A_2|A_2|^2(\hat{\Psi}_{14}+\hat{\Psi}_{15})\}. \quad (34)$$

Now we substitute these expansions into the governing equation, and consider successively the terms at $O(|(A_1,A_2)|^3)$ proportional to e^{iky}.

We find from the component proportional to $(R_2,S_2)A_1$ that

$$\mathbf{K}_0(k)(R_2\hat{\Psi}_9^{(R)}+S_2\hat{\Psi}_9^{(S)}) = -(R_2\mathbf{K}_R+S_2\mathbf{K}_S)\hat{\Psi}_1-\mu\mathbf{J}(k)\hat{\Psi}_2. \quad (35)$$

Since $\mathbf{K}_0(k)$ is singular then we must ensure that the right-hand side of this equation lies in the range of $\mathbf{K}_0(k)$. We achieve this by choosing μ to satisfy a solvability condition. To compute the appropriate value for μ we take the inner product of (35) with $\hat{\Psi}_1^\dagger$, the adjoint eigenfunction. This yields

$$\mu = -\langle\hat{\Psi}_1^\dagger, \mathbf{J}^{-1}(k)(R_2\mathbf{K}_R+S_2\mathbf{K}_S)\hat{\Psi}_1\rangle/\langle\hat{\Psi}_1^\dagger,\hat{\Psi}_2\rangle,$$

where as before $\langle\ \rangle$ denotes the inner product. Once μ is chosen in this way we calculate $\hat{\Psi}_9^{(R)}(z)$ and $\hat{\Psi}_9^{(S)}(z)$ to within a multiple of the zero eigenmode $\hat{\Psi}_1(z)$.

The component proportional to $(R_2,S_2)A_2$ gives

$$\mathbf{K}_0(k)(R_2\hat{\Psi}_{10}^{(R)}+S_2\hat{\Psi}_{10}^{(S)}) = -(R_2\mathbf{K}_R+S_2\mathbf{K}_S)\hat{\Psi}_2$$
$$-\mathbf{J}(k)(R_2\hat{\Psi}_9^{(R)}+S_2\hat{\Psi}_9^{(S)})-\nu\mathbf{J}(k)\hat{\Psi}_2.$$

The solvability condition is now that

$$\nu = -\langle\hat{\Psi}_1^\dagger, \mathbf{J}^{-1}(k)(R_2\mathbf{K}_R+S_2\mathbf{K}_S)\hat{\Psi}_2+(R_2\hat{\Psi}_9^{(R)}+S_2\hat{\Psi}_9^{(S)})\rangle/\langle\hat{\Psi}_1^\dagger,\hat{\Psi}_2\rangle.$$

The value of ν that we obtain is independent of the component of $\hat{\Psi}_1$ in $\hat{\Psi}_9^{(R)}$ and $\hat{\Psi}_9^{(S)}$ because $\langle\hat{\Psi}_1^\dagger,\hat{\Psi}_1\rangle = -\langle\hat{\Psi}_1^\dagger,\mathbf{J}^{-1}(k)\mathbf{K}_0(k)\hat{\Psi}_2\rangle = 0$. For the purposes of computing the coefficients in (24) there is no need to calculate $\hat{\Psi}_{10}^{(R)}$ or $\hat{\Psi}_{10}^{(S)}$.

Now we proceed to calculate the coefficients of the nonlinear terms in (24). The terms of order $A_1|A_1|^2$ satisfy

$$a\mathbf{J}(k)\hat{\Psi}_{12}+\mathbf{K}_0(k)\hat{\Psi}_{11} = \mathbf{N}(A_1|A_1|^2). \quad (36)$$

We find that a is given uniquely by a solvability condition, but $\hat{\Psi}_{11}$ is determined only up to a multiple of the complementary function, so that $\hat{\Psi}_{11} = \bar{\Psi}_{11}+\alpha_{11}\hat{\Psi}_1$, where $\langle\hat{\Psi}_1^\dagger,\bar{\Psi}_{11}\rangle = 0$, and we are free to choose the constant α_{11} as we wish.

Similarly, from

$$\mathbf{J}(k)(d\hat{\Psi}_{12}+2\hat{\Psi}_{11})+\mathbf{K}_0(k)\hat{\Psi}_{12} = \mathbf{N}(A_2|A_1|^2) \quad (37)$$

λ	Coefficients
0	$R^{\mathrm{D}} = 741.64, \quad S^{\mathrm{D}} = 72.01$ $\mu = 0.0407(R-R^{\mathrm{D}}) - 0.1596(S-S^{\mathrm{D}})$ $\nu = 0.0127(R-R^{\mathrm{D}}) - 0.0115(S-S^{\mathrm{D}})$ $a = 44.59, \quad b = 5.827, \quad c = -19.59, \quad d = -0.747$
1	$R^{\mathrm{D}} = 1825.35, \quad S^{\mathrm{D}} = 74.03$ $\mu = 0.0400(R-R^{\mathrm{D}}) - 0.1564(S-S^{\mathrm{D}})$ $\nu = 0.0125(R-R^{\mathrm{D}}) - 0.0115(S-S^{\mathrm{D}})$ $a = 45.02, \quad b = 7.431, \quad c = -20.77, \quad d = -1.213$
2	$R^{\mathrm{D}} = 3747.63, \quad S^{\mathrm{D}} = 79.22$ $\mu = 0.0384(R-R^{\mathrm{D}}) - 0.1491(S-S^{\mathrm{D}})$ $\nu = 0.0121(R-R^{\mathrm{D}}) - 0.0116(S-S^{\mathrm{D}})$ $a = 45.70, \quad b = 6.356, \quad c = -23.83, \quad d = -2.354$
4	$R^{\mathrm{D}} = 10678.68, \quad S^{\mathrm{D}} = 92.62$ $\mu = 0.0351(R-R^{\mathrm{D}}) - 0.1336(S-S^{\mathrm{D}})$ $\nu = 0.0112(R-R^{\mathrm{D}}) - 0.0117(S-S^{\mathrm{D}})$ $a = 45.38, \quad b = 20.28, \quad c = -31.15, \quad d = -4.904$

TABLE 1. Coefficients of the normal form (24) for various values of the Stokes-drift parameter, λ

we may find d uniquely. Then $\hat{\boldsymbol{\Psi}}_{12} = \bar{\boldsymbol{\Psi}}_{12} + 2\alpha_{11}\hat{\boldsymbol{\Psi}}_2 + \alpha_{12}\hat{\boldsymbol{\Psi}}_1$, where we specify that $\langle \hat{\boldsymbol{\Psi}}_1^{\dagger}, \bar{\boldsymbol{\Psi}}_{12} \rangle = 0$, and α_{12} is a constant at our disposal.

The constant c is determined uniquely from

$$\mathbf{J}(k)(c\hat{\boldsymbol{\Psi}}_{12} + \hat{\boldsymbol{\Psi}}_{11}) + \mathbf{K}_0(k)\hat{\boldsymbol{\Psi}}_{13} = \mathbf{N}(A_2^* A_1^2), \tag{38}$$

and $\hat{\boldsymbol{\Psi}}_{13} = \bar{\boldsymbol{\Psi}}_{13} + \alpha_{11}\hat{\boldsymbol{\Psi}}_2 + \alpha_{13}\hat{\boldsymbol{\Psi}}_1$.

Finally we compute the coefficient b from

$$\mathbf{J}(k)(b\hat{\boldsymbol{\Psi}}_{12} + \hat{\boldsymbol{\Psi}}_{12} + 2\hat{\boldsymbol{\Psi}}_{13}) + \mathbf{K}_0(k)\hat{\boldsymbol{\Psi}}_{14} = \mathbf{N}(A_1|A_2|^2). \tag{39}$$

Now, however, b depends on α_{11}. We choose $\alpha_{11} = 0$ for definiteness, and we note that the uniqueness of the constants a, c and d is a consequence of the 'minimal' normal form (24) that was chosen. The ambiguity in b (that is, its dependence on the exact definition of the amplitudes A_1 and A_2 through α_{11}) is reflected in Dangelmayr & Knobloch's analysis, where b does not figure in a significant way.

This is as far as we need to go in order to compute the coefficients in the amplitude equations. We find when we try to solve for $\hat{\boldsymbol{\Psi}}_{15}$ and $\hat{\boldsymbol{\Psi}}_{16}$ that α_{12} and $\alpha_{14} + \alpha_{15}$ must be chosen appropriately to satisfy solvability conditions. There remain three independent constants at our disposal in determining the cubic-order functions proportional to $\mathrm{e}^{\mathrm{i}ky}$, and these constants are fixed by our definitions of the amplitudes A_1 and A_2.

We find, using *Mathematica*, that the coefficients in (24) are as given in table 1.

4. Predictions from normal forms with $O(2)$ symmetry

4.1. *Predictions for steady and oscillatory bifurcations*

The first bifurcation of the basic state as R is increased is to steady convection when $S < S^{\mathrm{D}} \approx 72.01$, and to oscillatory convection, in a Hopf bifurcation, when $S > S^{\mathrm{D}}$. The bifurcation to steady convection is supercritical when $S < S^* \approx 13.8$, and

S	R_c	$Nu-1$
0	458.79	$0.0424R_2-0.167S_2$
8	490.26	$0.102R_2-0.398S_2$
13.2	510.71	$1.003R_2-3.946S_2$
13.79	513.03	$-100.2R_2+394.1S_2$
14	513.85	$-2.716R_2+10.68S_2$
20	537.44	$0.0945R_2+0.371S_2$

TABLE 2. Nusselt number near the steady bifurcation of the basic state predicted by weakly nonlinear analysis. The graph of Nusselt number against $R-R_c$ (for fixed S) becomes very steep (and indeed vertical) at the changeover between supercritical and subcritical bifurcation.

S	R^H	$Nu-1$	Phase speed, c
120	783.90	$0.0986R_2-0.0868S_2$	$0.7672-0.0442R_2+0.0469S_2$
150	810.27	$0.0783R_2-0.0688S_2$	$0.9787-0.0342R_2+0.0363S_2$
200	854.17	$0.0580R_2-0.0509S_2$	$1.255-0.0260R_2+0.0278S_2$
450	1072.54	$0.0247R_2-0.0215S_2$	$2.167-0.0138R_2+0.0149S_2$
3000	3191.63	$0.00255R_2-0.00202S_2$	$6.303-0.00364R_2+0.00406S_2$

TABLE 3. Weakly nonlinear prediction of the Nusselt number and phase speed, c, for the travelling wave branch close to the Hopf bifurcation at $R = R^H$, for various values of the stratification parameter, S. This branch exists only when there are periodic lateral boundary conditions (in which case it is stable).

subcritical when $S > S^*$. At the Hopf bifurcation, both TW and SW bifurcate supercritically, with the TW of larger amplitude, and stable. The SW are unstable.

From our weakly nonlinear analysis we may compute various quantities of interest, for example the Nusselt number (Nu), a dimensionless measure of the heat flux through the upper surface of the fluid layer. With an angle bracket denoting a y-average,

$$Nu-1 = \left\langle \frac{\partial\theta}{\partial z}(y,0,t) \right\rangle.$$

We show in §5 how the results of the analysis compare with our direct numerical integrations of the PDEs.

In table 2 we show the Nusselt number predictions near the bifurcation to steady convection, for a variety of values of the stratification parameter, S. In each case, $Nu-1$ is proportional to the distance in parameter space from the steady bifurcation point, $R = R_c$. In fact our numerical integrations are for fixed values of S, and with increasing R, so that the predictions for our simulations result from setting $S_2 = 0$. For completeness, though, we have given results that allow a more general displacement from the bifurcation point in parameter space. That the bifurcation is supercritical for $S < S^* \approx 13.8$ and subcritical for $S > S^*$ can be seen in the values of the Nusselt number, as the curve of $Nu-1$ against $R-R_c$ (for fixed S) becomes vertical at the changeover.

Tables 3 and 4 show some predictions of the weakly nonlinear theory for the oscillatory bifurcation of the basic state that occurs for $S > S^D$. The Nusselt number for the TW convection and its phase speed are indicated in table 3, and the Nusselt number and frequency of the SW are indicated in table 4. We recall that the TW is stable with lateral boundary conditions, and the SW is stable only for flux-free

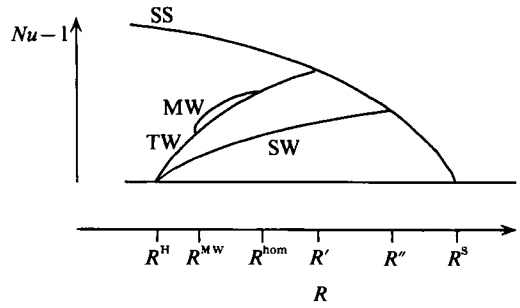

FIGURE 2. Bifurcation diagram predicted by the weakly nonlinear analysis of the Takens–Bogdanov bifurcation with $O(2)$ symmetry, for values of the Stokes-drift parameter $\lambda = 0, 1, 2, 4$, and presumably for intermediate values also. The stratification parameter S is a little above S^{D}, and R increases to the right. The diagram is selected from the classification of Dangelmayr & Knobloch (1987). Note that here the modulated wave (MW) is indicated by a representative average Nusselt number over its cycle, whereas later in our numerical results we plot instead the maximum and minimum values achieved by the Nusselt number over the MW cycle. The various values of R indicate the Hopf bifurcation (R^{H}) of the basic state, the steady bifurcation (R^{S}), the birth and death of the modulated waves (R^{MW} and R^{hom}, respectively) and the terminations of the TW and SW branches (R' and R'', respectively).

S	$Nu-1$	Frequency, ω
120	$(0.00641R_2-0.00564S_2)(1+1.005\sin 2\omega t)$	$2.410-0.0174R_2+0.0404S_2$
150	$(0.00610R_2-0.00536S_2)(1+1.008\sin 2\omega t)$	$3.075-0.0139R_2+0.0319S_2$
200	$(0.00566R_2-0.00496S_2)(1+1.013\sin 2\omega t)$	$3.942-0.0110R_2+0.0251S_2$
450	$(0.00426R_2-0.00370S_2)(1+1.035\sin 2\omega t)$	$6.807-0.00660R_2+0.0149S_2$
3000	$(0.00109R_2-0.000867S_2)(1+1.0824\sin 2\omega t)$	$19.80-0.00259R_2+0.00575S_2$

TABLE 4. Weakly nonlinear prediction of the Nusselt number and frequency, ω, for the standing wave branch close to the Hopf bifurcation, for various values of the stratification parameter, S. This branch is stable only when flux-free lateral boundary conditions are imposed. The values of R at which the Hopf bifurcation occurs are given in table 3.

lateral boundaries. Note that $Nu-1 < 0$ for part of the SW cycle, consistent with direct numerical integrations of the partial differential equations close to the bifurcation point. This phenomenon is explored in detail by Cox *et al.* (1992).

4.2. *Predictions from the double-zero normal form*

Dangelmayr & Knobloch (1987) describe all possible bifurcation diagrams that can result from the normal form (24) as the unfolding parameters μ and ν are varied. There are many cases, according to the coefficients of the nonlinear terms. The values we have computed for various λ, which are displayed in table 1, indicate that for $\lambda = 0, 1, 2, 4$ (and presumably for intermediate values also) the relevant case is '$II-(A > 0)$' (Dangelmayr & Knobloch 1987). We reproduce the appropriate bifurcation diagram in figure 2. In terms of our parameters R and S, the implications of this diagram are as follows.

For each λ there is a critical value of the stratification parameter, $S^{D}(\lambda)$, such that for $S < S^{D}(\lambda)$ the basic state becomes unstable to steady convection in a subcritical bifurcation, as R is increased (Arrow A in figure 3 shows this bifurcation). (This fact is consistent with our analyses of the steady and Hopf bifurcations individually. Note that the double-zero analysis does not predict the supercritical steady

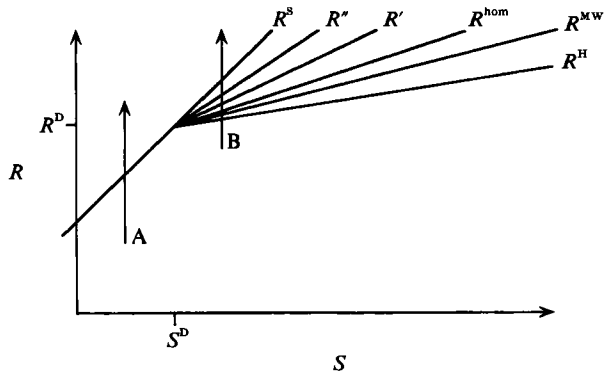

FIGURE 3. The bifurcation of the basic state for $S < S^D$ as R is increased is indicated by arrow A: there is a subcritical steady bifurcation. Arrow B indicates the more complicated sequence of bifurcations when $S > S^D$, as shown in figure 2. As this arrow cuts the various lines indicated, the corresponding bifurcations shown in figure 2 occur.

convection that we find for small S – these values of S are too far from the double-zero point for that analysis to be relevant.) For $S > S^D(\lambda)$ the basic state loses stability to oscillatory convection. As we already know from the analysis of this Hopf bifurcation, and is predicted also by the double-zero analysis, both TW and SW bifurcate supercritically, but with only the TW stable (see figure 2). As R is increased through R^{MW} the TW undergoes a Hopf-bifurcation at which it becomes unstable, and a stable branch of modulated waves (MW) arises. These MW exist over a finite interval in R (and exist arbitrarily close to the double-zero point), and cease to exist when they become homoclinic to the TW branch, when $R = R^{hom}(\lambda, S)$, say. For $R > R^{hom}$, no stable states are predicted by this analysis. In practice we expect quintic terms in the normal form to stabilize the steady states (SS) in a turning point, so that there are stable large-amplitude SS that will be found for $R > R^{hom}$. Arrow B in figure 3 shows the sequence of bifurcations in parameter space.

In fact, for a qualitative description of the dynamics we did not need to compute the coefficients in (24) because the only region of Dangelmayr & Knobloch's (1987) parameter space consistent with the information we have about the individual steady and Hopf bifurcations is '$II-(A > 0)$'. We can, however, use these coefficients to make quantitative predictions from the amplitude equations, in particular about the existence of modulated waves. Dangelmayr & Knobloch show that MW can be expected between two half-lines in parameter space which they call SL_M and L_H, where

$$SL_M : a\nu = \frac{2dm\mu}{3m-5d}; \quad \mu < 0, \tag{40}$$

$$L_H : \mu = \left(\frac{3m-d}{2m-4d}\right)\frac{a}{d}\nu; \quad \mu < \frac{a}{d}\nu, \tag{41}$$

and $m = 2c+d$. In the present problem, in (R_2, S_2)-parameter space, these half-lines turn out to be

$$\left.\begin{aligned} SL_M : R_2 &= 1.12S_2; \quad R_2, S_2 > 0, \\ L_H : R_2 &= 1.08S_2; \quad R_2, S_2 > 0, \end{aligned}\right\} \tag{42}$$

so they form a wedge of angle approximately 1°. Thus the range of parameters near the Takens–Bogdanov point where MW exist (and are stable) is tiny. As we move

further in parameter space from the double-zero point we expect the multiple bifurcation analysis to become less relevant, and the analysis of the separate bifurcations to steady and oscillatory convection to become correspondingly more relevant (for example, predicting supercritical steady bifurcation for small S).

5. Solution symmetries

In this section we list some of the symmetries exhibited by the SS, TW and SW states that we compute. We describe the symmetries that we expect from the weakly nonlinear calculations, and say whether the numerically computed states, to be described further in the next section, in fact exhibit these symmetries.

We note here that LLM found some TW states that were reported to have no stagger in the position of their cell centres. We find these to be 'impossibly symmetric' because when TW bifurcate from the basic state they demonstrably have staggered cell centres. Indeed, this observation was the motivation for the present section. (By 'cell centre' we mean, as appropriate, the maximum or minimum of the stream function in the cell.)

5.1. *Steady states*

The eigenfunctions of the linear problem take the form

$$\psi = \hat{\psi}(z)\sin ky, \quad u = \hat{u}(z)\cos ky, \quad \theta = \hat{\theta}(z)\cos ky,$$

where the y origin is suitably chosen, and $\hat{\psi}$, $\hat{u}$, $\hat{\theta}$ are even functions of $z+\frac{1}{2}$. A weakly nonlinear expansion of the steady states near their bifurcation from the basic state yields solutions with the following symmetries:

(i) reflection in a cell wall: $y \mapsto -y$, $\psi \mapsto -\psi$, $u \mapsto u$, $\theta \mapsto \theta$;
(ii) 'flip symmetry': $y \mapsto y+\pi/k$, $z \mapsto -1-z$, $\psi \mapsto -\psi$, $u \mapsto -u$, $\theta \mapsto -\theta$;
(iii) point symmetry about centre of cell: $y \mapsto \pi/k-y$, $z \mapsto -1-z$, $\psi \mapsto \psi$, $u \mapsto -u$, $\theta \mapsto -\theta$.

Provided the linear eigenfunction does not represent cells stacked vertically (this is true for the steady bifurcations we analyse in this paper), and provided the cells have just one centre, then the point symmetry 3 requires that the cell centre lies on the midline $z = -\frac{1}{2}$. For 'staggered' cell centres (which lie alternately above and below the midline), the point symmetry must be broken.

In all of the stable steady states we have computed numerically the three symmetries have been present. In particular, the cell walls are always vertical and the cell centres lie on $z = -\frac{1}{2}$.

5.2. *Travelling waves*

The travelling wave eigenfunction takes the form $\psi = \hat{\psi}_a(z)\sin(ky-\omega t-\hat{\psi}_p(z))$, $u = \hat{u}_a(z)\cos(ky-\omega t-\hat{u}_p(z))$, $\theta = \hat{\theta}_a(z)\cos(ky-\omega t-\hat{\theta}_p(z))$, where $\hat{\psi}_{a,p}$, $\hat{u}_{a,p}$, $\hat{\theta}_{a,p}$, are even functions of $z+\frac{1}{2}$. In general the phases of $\hat{\psi}_p$, $\hat{u}_p$, $\hat{\theta}_p$, are all different, and so the eigenfunction has the following symmetries:

(i) translation by half wavelength: $y \mapsto y+\pi/k$, $\psi \mapsto -\psi$, $u \mapsto -u$, $\theta \mapsto -\theta$;
(ii) reflection about midline: $z \mapsto -1-z$, $\psi \mapsto \psi$, $u \mapsto u$, $\theta \mapsto \theta$.

The weakly nonlinear travelling waves preserve these symmetries only in the combination

(iii) 'flip symmetry': $y \mapsto y+\pi/k$, $z \mapsto -1-z$, $\psi \mapsto -\psi$, $u \mapsto -u$, $\theta \mapsto -\theta$.

In particular the weakly nonlinear travelling wave does not have vertical cell walls, and its cell centres are staggered.

In our numerical simulations of the full PDEs we find no travelling waves for which this 'flip symmetry' is broken. (In contrast with LLM, we do not find the two distinct types of travelling wave, TW1 and TW2, for large values of the stratification parameter, S, nor do we find any 'two-centred' TW cells.)

5.3. *Standing waves*

The linear standing waves are of the form

$$\psi = \hat{\psi}_a(z)\sin(\omega t+\hat{\phi}_\psi(z))\sin ky, \quad u = \hat{u}_a(z)\sin(\omega t+\hat{\phi}_u(z))\cos ky,$$
$$\theta = \hat{\theta}_a(z)\sin(\omega t+\hat{\phi}_\theta(z))\cos ky,$$

where each amplitude (a) and phase ($\hat{\phi}$) is an even function of $z+\frac{1}{2}$. The weakly nonlinear standing waves exhibit the following spatial symmetries:

(i) reflection in a cell wall: $y\mapsto -y$, $\psi\mapsto -\psi$, $u\mapsto u$, $\theta\mapsto\theta$;
(ii) 'flip symmetry': $y\mapsto y+\pi/k$, $z\mapsto -1-z$, $\psi\mapsto -\psi$, $u\mapsto -u$, $\theta\mapsto -\theta$;
(iii) point symmetry about centre of cell: $y\mapsto \pi/k-y$, $z\mapsto -1-z$, $\psi\mapsto\psi$, $u\mapsto -u$, $\theta\mapsto -\theta$.

Also there is the temporal/spatial symmetry

(iv) advancing time by one half-period, and reflection about midline: $t\mapsto t+\pi/\omega$, $z\mapsto -1-z$, $\psi\mapsto -\psi$, $u\mapsto -u$, $\theta\mapsto -\theta$;

The phase functions $\hat{\phi}$, result in the splitting of each convection cell into vertically stacked cells during a small fraction of the SW cycle at which the convective energy is smallest (see Cox *et al.* 1992).

6. Simulation

6.1. *Quantitative comparison between PDE's and weakly nonlinear theory*

We find good agreement between our weakly nonlinear results and our numerical results, as we summarize below.

At $S = 0$, our weakly nonlinear analysis predicts a supercritical bifurcation to steady convection, with

$$Nu-1 = 0.04237(R-R_c)+O((R-R_c)^2),$$

where $R_c \approx 458.790$. A least-squares fit of the Nusselt number calculated for the PDEs at $R = 463.8$, 465, and 480 gives

$$Nu-1 = 0.0422(R-R_c)-0.0008(R-R_c)^2+0.00001(R-R_c)^3,$$

which is in excellent quantitative agreement with the weakly nonlinear prediction. As table 5 shows, however, the values of $Nu-1$ rapidly diverge as one moves away from the bifurcation point.

At $S = 350$, where the Hopf bifurcation is at $R_c = 985.42$, the weakly nonlinear analysis predicts for TW,

$$Nu-1 = 0.03220(R-R_c)+O((R-R_c)^2).$$

	$Nu-1$	
R	w.n. prediction	PDE integration
463.8	0.2123	0.1928
465	0.2632	0.2340
480	0.8987	0.6388
520	2.5935	1.2518

TABLE 5. Nusselt numbers close to the bifurcation of the SS for $S = 0$. The weakly nonlinear prediction (w.n.) tends to overestimate the Nusselt number computed by direct numerical integration of the PDEs. The critical value of R is $R_c \approx 458.79$.

	$Nu-1$	
R	w.n. prediction	PDE integration
987	0.0509	0.0510
990	0.1475	0.1242
1000	0.4695	0.3149

TABLE 6. Nusselt numbers close to the bifurcation of the TW for $S = 350$. The weakly nonlinear theory tends to overestimate the Nusselt number computed directly from the PDEs. The critical value of R is $R_c \approx 985.42$.

A fit of the data from the PDE integrations at $R = 987$ and 990 gives

$$Nu-1 = 0.0350(R-R_c)-0.001\,73(R-R_c)^2,$$

which is in reasonable agreement. Table 6 shows the details of our comparison.

We observe that the criticality must be quite small, $(R-R_c)/R_c \sim 0.01$, to get a good quantitative fit between the weakly nonlinear analysis and the direct numerical integrations of the PDEs. On the other hand, it will be seen that the qualitative predictions of the analysis are indeed in accord with numerical simulation over a substantial portion of the parameter range explored here.

6.2. *Integration in a finite box*

We note here that because we quantize the wavenumber k by integrating over a finite interval in y we ignore a continuum of unstable modes in our integrations. When we fix $L = 2$ so that the fundamental wavenumber is $k = \pi$, we ignore all the modes with $k < \pi$, which are unstable. The existence of these unstable modes is a consequence of the zero critical wavenumber, and the infinite horizontal extent of motions at onset, which in turn is a consequence of our modelling of the upper and lower boundaries of the fluid layer as stress-free. If a more involved modelling of these boundaries is undertaken, which incorporates the reduction in the applied wind stress when the differential in the speed of the wind and the surface water decreases, then there is a finite critical wavelength, and the problem of arbitrarily choosing a horizontal lengthscale is obviated (Cox & Leibovich 1992).

6.3. *Numerical integrations*

When $S = 0$ we find a branch of steady states that arises from the supercritical steady bifurcation at $R_c \approx 458.79$. We have computed this branch for $R_c < R < 2000$ – the SS are apparently the only stable states for the unstratified problem over this range

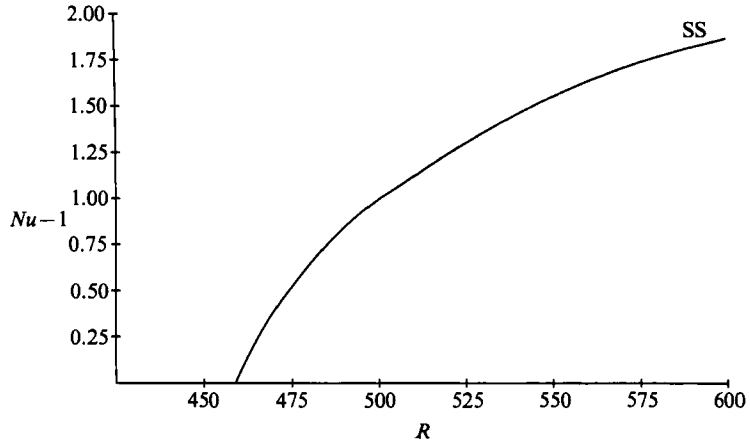

FIGURE 4. Nusselt number as a function of R for $S = 0$, from direct numerical simulation of the governing PDEs. This SS branch is the only branch of solutions we find.

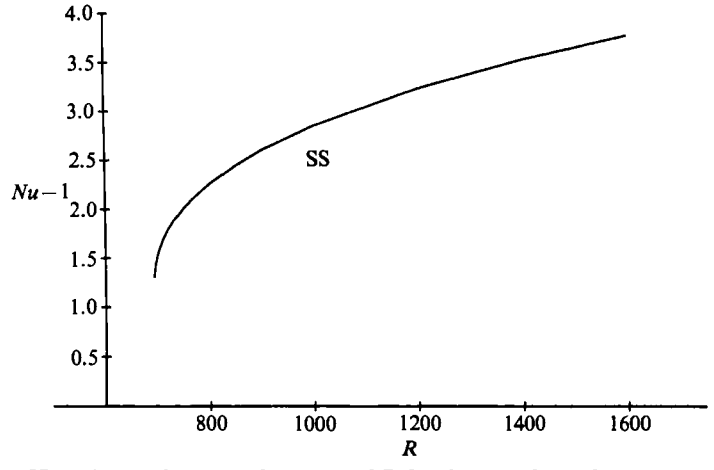

FIGURE 5. Nusselt number as a function of R for $S = 80$, from direct numerical simulation of the governing PDEs.

of R. Figure 4 shows the plot of Nusselt number against R. We observe that these SS retain vertical flux-free cell walls at which $\psi = \psi_{yy} = u_y = \theta_y = 0$, and so they also solve the flux-free problem.

For $S = 80$ (a value greater than S^{D}, so the first bifurcation of the basic state is to oscillatory convection, at $R_c \approx 748.69$) we find only large-amplitude SS for a variety of initial conditions and a range of R, including values subcritical to the steady bifurcation at $R_c \approx 772.63$. We estimate that the turning point of the SS branch occurs at $R \approx 690$. We infer the existence of an unstable branch of SS linking the turning point to the steady bifurcation point. We infer also that the TW and MW branches of figure 2 could in principle be computed, but that they have such a small region of stability that we have been unable to find appropriate initial conditions for the numerical simulations to evolve to these oscillatory states. Figure 5 shows the plot of Nusselt number against R.

For $S = 120$ the subcritical branch of SS does not mask the oscillatory solutions. We find stable TW that bifurcate supercritically from the basic state in the Hopf

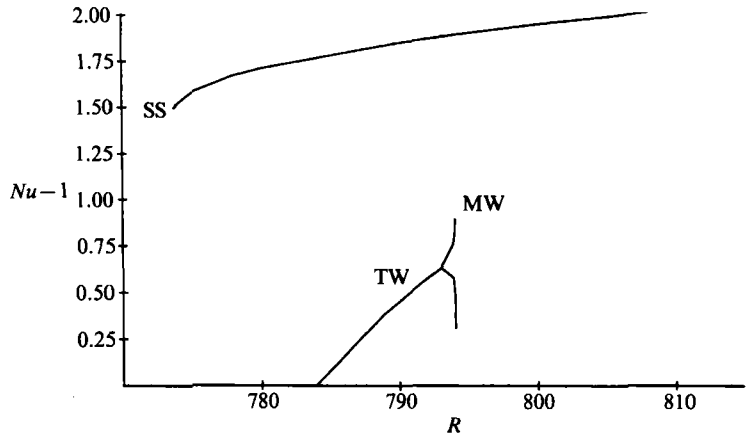

FIGURE 6. Nusselt number as a function of R for $S = 120$, from direct numerical simulation of the governing PDEs. Marked are the branches of steady states, travelling waves and modulated travelling waves. The MW branch is indicated by two curves, one denoting the maximum value of the Nusselt number achieved over one cycle, and the other denoting the minimum.

bifurcation at $R_c \approx 783.90$ and also, for a small range of R, MW that bifurcate from the TW in secondary Hopf bifurcation at $R \approx 792$, and cease to exist when $R \approx 794.04$. Figure 6 shows the three branches of solutions – note that the MW branch is indicated by two curves, one each for the maximum and minimum value of $Nu-1$ over the cycle. We may compare the region of existence of the MW with the prediction based on the weakly nonlinear analysis: since $S = 120$, then $S-S^D \approx 48$, and the MW are born when $R-R^D \approx 50.4((R-R^D)/(S-S^D) \approx 1.05)$ and they die when $R-R^D \approx 52.4((R-R^D)/(S-S^D) \approx 1.11)$. This is in good agreement with the prediction (42), considering that this example is far from criticality. The large-amplitude branch of SS appears to be the only stable state for $R > 794.04$. It can be continued back to $R \approx 773.8$, a value subcritical to both the Hopf and steady bifurcations of the basic state. For $S = 150$ the bifurcation diagram is similar, but the oscillations of the MW reach larger amplitude before the MW branch disappears. The MW again exist over a very small range in R, but a larger range than for $S = 120$. The way in which the MW cease to exist is not clear from our integrations at either $S = 120$ or $S = 150$. The turning point, or 'knee', in the SS branch where this solution becomes stable occurs for larger R as S is increased, that is, it moves to the right in the bifurcation diagrams.

When $S = 200$ (figure 7) we again find a stable TW branch born from a supercritical Hopf bifurcation of the basic state, at $R_c \approx 854.17$. This TW branch loses stability in a secondary Hopf bifurcation to MW, when $R \approx 908$. The MW do not terminate in a homoclinic bifurcation to the TW branch as predicted by the Takens–Bogdanov normal form, but seem to become heteroclinic to the SS and the SW solutions. (The branch of steady states has moved further to the right; for example the turning point is at $R \approx 917.5$.) In order to describe the MW near this heteroclinic bifurcation, we find it convenient to picture the MW solution as evolving with time in phase space. Because it has two frequencies, the MW traces out a trajectory on a torus as it evolves. The behaviour of this trajectory near the global bifurcation is as follows. It begins close to a SS solution, which is reflectionally symmetric (that is, it lies in the Z_2-invariant subspace). This SS is, however, unstable to Z_2-symmetric SW perturbations and so the trajectory leaves the neighbourhood

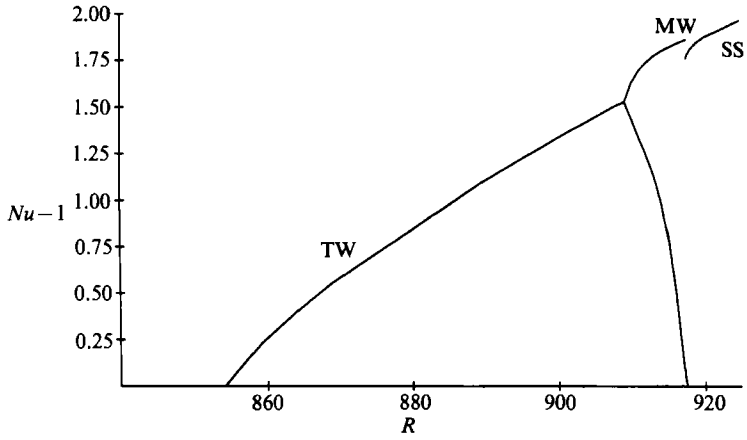

FIGURE 7. Nusselt number as a function of R for $S = 200$, from direct numerical simulation of the governing PDEs. The branches of SS, TW and MW are indicated.

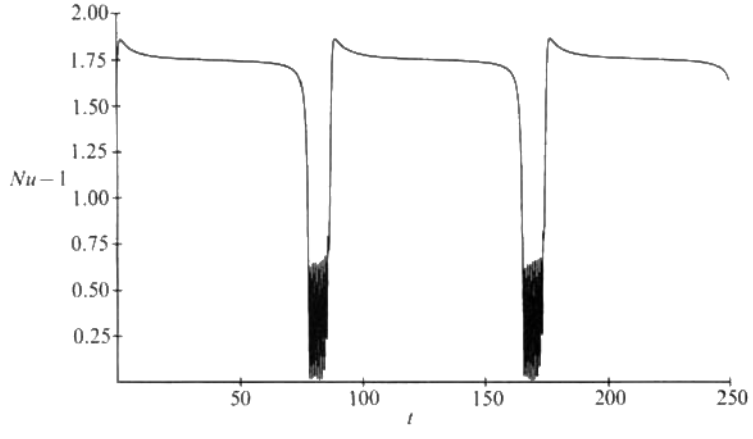

FIGURE 8. Nusselt number plotted against time, t, for the MW solution near its heteroclinic bifurcation with the unstable SS and SW solutions. The unstable SS has $Nu - 1 \approx 1.76$, which we identify with the long quasi-steady portion of the Nusselt-number time trace.

of the SS and approaches a SW solution. This SW has the same phase as the SS, that is, the cell boundaries of the rolls in the SW are at the same y location as for the SS solution. The MW does not approach the SW indefinitely, because it does not lie exactly in the Z_2-invariant subspace. In the neighbourhood of the SW the MW experiences an exponential growth of TW perturbations, which break the Z_2-symmetry. The TW are of considerably larger amplitude than the SW, but are unstable and so the trajectory proceeds again into a neighbourhood of an SS solution. The phase of this new SS is not in general the same as during the previous passage of the trajectory near the SS because the TW episode shifts the phase. (So in fact for the periodic problem when we talk of the SS branch, we mean that there is a circle of SS, with all possible phases. Similarly there is a circle of SW, each with different phase.) This phase shift is the same on each passage of the trajectory around the MW torus, although we have not attempted to demonstrate this last fact from our numerical solutions. Figure 8 shows the time trace of $Nu - 1$ for the MW near its heteroclinic bifurcation. The long quasi-constant segment and the oscillations represent the MW's sojourn near the unstable SS and SW, respectively.

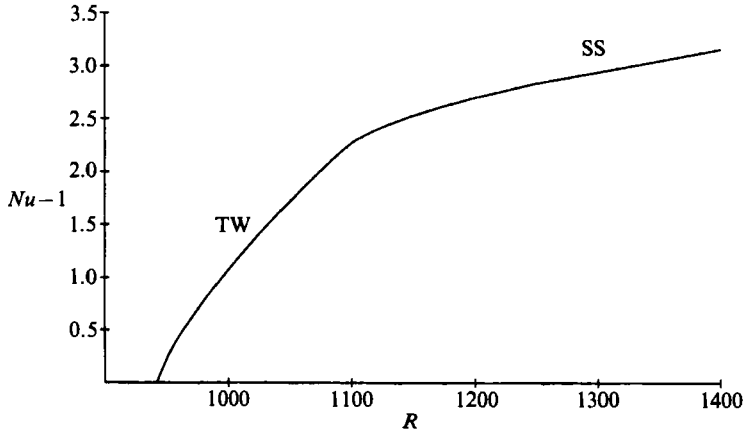

FIGURE 9. Nusselt number as a function of R for $S = 300$, from direct numerical simulation of the governing PDEs. Indicated are the branches of TW and SS.

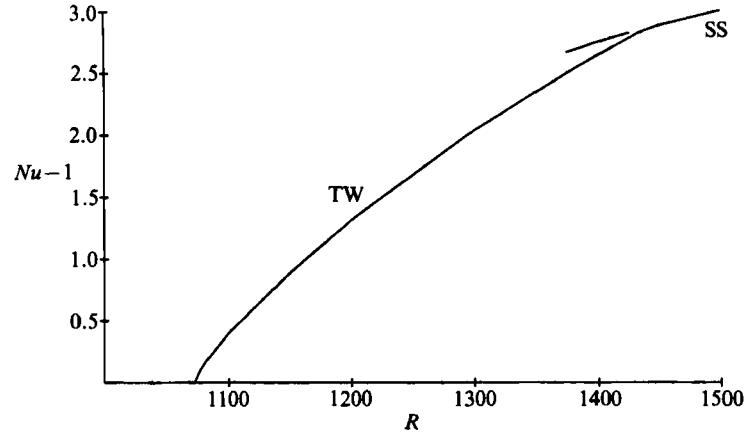

FIGURE 10. Nusselt number as a function of R for $S = 450$, from direct numerical simulation of the governing PDEs. Indicated are the branches of TW and SS. The disjoint line to the right of the stable branch marks unstable SS that have been computed as described in the text.

The bifurcation diagram for $S = 300$ (figure 9) is unlike those described above: there is no bifurcation to MW on the TW branch, but there seems to be a direct bifurcation involving the TW and SS branches at $R \approx 1100$. The TW branch joins to the SS branch above the SS turning point, so that now the SS does not gain stability at its turning point, but later at its bifurcation with the TW branch. For $941.75 \approx R_c < R < 1100$ we find only TW, while for $1100 < R < 1600$ we find only SS.

The bifurcation diagram for $S = 450$ (figure 10) is similar to that at $S = 300$: the TW branch (born at $R_c \approx 1072.54$) does not undergo the Hopf bifurcation to MW, and the bifurcation involving the TW and SS branches occurs above the turning point of the SS. We find only TW for $R_c < R < 1436$, and only SS for $1436 < R < 1600$. (We are, fortunately, able to calculate some unstable SS to a high degree of accuracy as follows. We take as an initial condition S_1, a stable SS that has already been calculated for a value of $R > 1436$, and integrate forwards in time. If the initial condition was exact, and if the numerical code integrated the governing equations exactly, then the solution would retain its Z_2 symmetry and approach an unstable steady state, S_∞, as $t \to \infty$. This steady state is a saddle, and S_1 lies on its

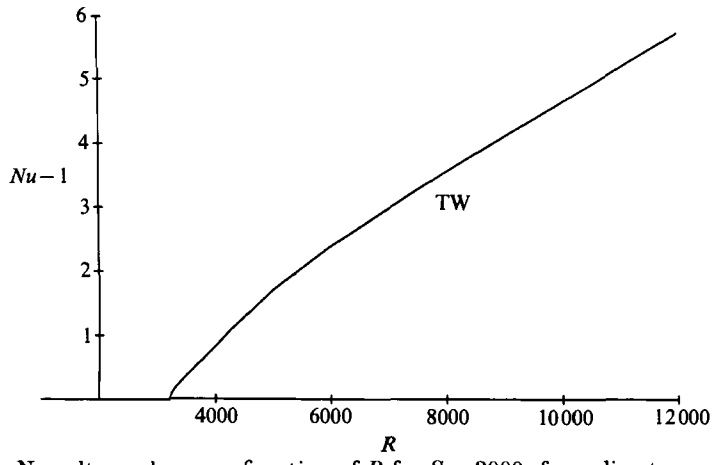

FIGURE 11. Nusselt number as a function of R for $S = 3000$, from direct numerical simulation of the governing PDEs. This branch of TW is the only branch of solutions we find.

stable manifold. However, numerical errors in the initial condition and in the integrations introduce non-Z_2-symmetric perturbations that force the evolving solution away from the stable manifold of S_∞, and in our case apparently onto the stable manifold of the TW. In practice we find that the solution remains close to the unstable SS for sufficiently long times that we can accurately determine, for example, the Nusselt number of the SS.) The bifurcation diagram at $S = 750$ seems similar, but we have less detail.

When $S = 3000$ we find only TW, for R up to 12000. It is not clear whether the branch of SS is unstable for all R or whether it stabilizes at some value of $R > 12000$. Figure 11 shows the plot of Nusselt number against R.

6.4. *Comparison between PDE integrations and results of Knobloch & Moore*

Knobloch & Moore (1990*a*, *b*) treat the problem of binary fluid convection between stress-free boundaries of fixed temperature and concentration, with $O(2)$ symmetry. Their governing PDEs are directly analogous to those governing two-dimensional Langmuir circulations, although their boundary conditions are not. For their system, like ours, there is a Takens–Bogdanov bifurcation that serves to organize the dynamics over a broad range of parameter values. The bifurcation to TW, however, is degenerate ($d = 0$ in (24)) and quintic terms must be included in the amplitude equations to determine the bifurcation picture. Knobloch & Moore derive a set of nine (complex) coupled ODEs that captures the dynamics of the PDEs near the Takens–Bogdanov point exactly, and they compare numerical integrations of this 'minimal model' with the *non-degenerate* amplitude equations. (They assume that the analysis of (24) with $d = 0$ should be similar to that with either small $d > 0$ or $d < 0$.) The resulting sequence of bifurcation diagrams for increasing S is remarkably similar to our own for the LC problem, although they are able to investigate their ODEs in greater numerical detail than we can our PDEs. They observe the approach of the MW to a heteroclinic orbit connecting solutions of the SW and SS branches, and demonstrate that the MW can exist only when the termination of the TW branch on the SS branch lies below the 'knee' of the SS branch. This observation is consistent with our results: for example, when $S = 200$ we find the TW → MW bifurcation, but when $S = 300$ we find no MW, and the TW terminates above the SS knee.

7. Conclusions

In this paper, the first quantitative comparison between direct numerical simulations and weakly nonlinear theory for $O(2)$ symmetric bifurcation problems is made. Many of the results were originally obtained by the weakly nonlinear analysis, and were observed to be inconsistent with the numerical results of LLM. This led us to a complete re-examination of the numerical results of LLM by an entirely different algorithm. Although the origin of the systematic numerical errors in LLM has yet to be identified, the excellent agreement of theory and numerical simulation found here give us the confidence to conclude that the present results are correct, while those of LLM are incorrect.

The mathematical analogy that exists (for $\lambda = 0$, or constant Stokes drift gradient) between the two-dimesional Langmuir circulation problem and thermohaline problems was the source of a surprising conclusion of LLM. A natural boundary condition in the Langmuir circulation problem corresponds in the thermohaline analogy to the imposition of constant-heat-flux boundary conditions, which differs from the best-studied thermohaline problem which imposes isothermal boundary conditions. This seems a rather innocent alternative, yet LLM found that the dynamics and the bifurcation sequences in the two cases were qualitatively different. This conclusion is now seen to be incorrect. The current paper demonstrates that qualitatively the problems are not much different, at least for the parameter regime explored here.

Weakly nonlinear analysis turns out to provide very accurate quantitative solutions when the departure from criticality is small ($R/R_c - 1 = O(10^{-2})$), but the correct qualitative behaviour is predicted over a much larger region. In this problem with periodic boundary conditions imposed, the modestly supercritical stable states are either travelling waves, modulated travelling waves, or steady states. Modulated travelling waves are 'fragile', in the sense that they are predicted to exist, and found in simulations to exist, in very small regions in parameter space. The 'robust' stable states are TW and SS. Weakly nonlinear theory valid to cubic order does not capture the stable SS when $S > S^*$. It therefore fails qualitatively to predict the system behaviour for those portions of the (S, R)-plane for $S > S^*$ for which the SS is the only stable motion. As S increases, the transition from an oscillatory to a steady state is deferred to larger values of $R/R_c - 1$ – for example, at $S = 3000$, the transition was not observed to occur for R/R_c as high as 4, and so the qualitative value of the weakly nonlinear prediction improves as S increases. The physical origin of this seems clear. Once the convective activity is sufficiently strong to effect substantial overturning and mixing, the effects of stratification are erased and the system behaves like a homogeneous fluid. No stable restoring force then exists and the anticipated convective motion is a steady state. As the stabilizing stratification (level of S) is increased, the vigour of convection (level of R) required to homogenize the water column increases.

The present results are limited to constant Stokes drift gradient. Exponential variations of Stokes drift are also treated here by weakly nonlinear theory. No qualitative changes in the bifurcation picture emerge as a result of this extension, for the range of exponential decay constants examined.

The prevalence of steady states or travelling waves is consistent with observations of Langmuir circulations, which show persistent windrows which sometimes drift at right angles to the wind direction. Preliminary computations with a three-dimensional code, which we hope to present in due course, show that rolls parallel to

the wind are the most unstable disturbance mode for unstratified water. Stable stratification, however, causes the most unstable (linear) modes to rotate from the wind direction. This effect does not seem to be a strong one, however, so the assumption of two-dimensional motion, made here, remains reasonable.

This work was supported by NSF OCE-9017882, NSF AM-88-14553, and AFOSR-89-0226. Support was also provided by a NATO Collaboration Research grant to S.L. and I.M.M. This research was conducted using the computational resources of the Cornell Theory Center, which receives major funding from the National Science Foundation and IBM Corporation, with additional support from New York State Science and Technology Foundation and members of the Corporate Research Institute.

Appendix A. Corrections to LLM

In this Appendix we summarize the errors in LLM: in the first section for the integrations under periodic lateral boundary conditions, and in the second section under flux-free boundary conditions. The present results supersede those of LLM.

A.1. *Periodic boundary conditions*

Under periodic boundary conditions, and for $L = 2$, the Nusselt numbers computed by LLM are consistently substantially overestimated. For example, for the unstratified case $S = 0$ we calculate that $Nu - 1 = 0.1928$ when $R = 463.8$, while it is 1.2 from figure 3 (a) of LLM. At $R = 480$ our simulations yield $Nu - 1 = 0.6388$, while the measured value from LLM is 2.8. The corresponding values to be contrasted at $R = 520$ are 1.2518 and 5.2 respectively. It is no longer true that the 'only time-dependent asymptotic states found are single-frequency periodic motions arising from the Hopf bifurcation' (LLM), for our integrations reveal the existence of two-frequency modulated waves, albeit over a very small range of parameters.

The slanted sidewalls shown for the SS for large S are a product of the numerical errors: we find that the SS always have vertical cell walls (both in plots of stream function and of vorticity).

The bifurcation picture that LLM find is considerably more complicated than we predict from our weakly nonlinear analysis and confirm with our direct numerical simulations. In particular, LLM report subcritical TW, co-existing stable SW and TW, and two distinct families of TW, which they call TW1 and TW2. The former family has solutions whose cell centres (that is, whose maxima and minima of the stream function) are offset from the horizontal midplane, while the latter has unstaggered cell centres. We find none of these phenomena: the Hopf bifurcation always gives supercritical TW and SW, with the former stable and the latter unstable. Accordingly, we never observe co-existing stable TW and SW, and we find only one family of TW, which always has staggered cell centres.

A.2. *Flux-free boundary conditions*

The results presented in LLM for flux-free boundary conditions overestimate the Nusselt number for all cases that have been compared.

For $S > S^{\mathrm{D}} \approx 72.01$, we find the first bifurcation of the basic state to be a Hopf bifurcation, giving an SW whose period increases with increasing R. This SW is destroyed in a global bifurcation where it becomes heteroclinic to a steady solution. This bifurcation occurs when $R = R^{\mathrm{het}}(S)$, say, and is indicated by the period of the

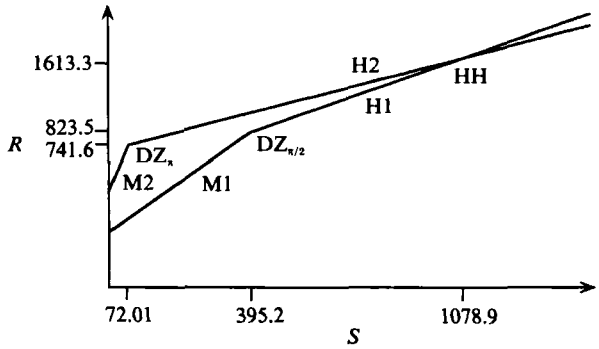

FIGURE 12. Stability diagram for $L = 4$. M indicates transition to monotonic convection, H a Hopf bifurcation to oscillatory convection. 1 indicates a bifurcation of the mode with wavenumber $\frac{1}{2}\pi$, 2 the mode with wavenumber π. The intersections of the monotonic and oscillatory bifurcation curves, the double-zero bifurcations, are indicated by DZ. The simultaneous Hopf bifurcation of $\frac{1}{2}\pi$ and π modes is indicated by HH.

SW becoming infinite. The values of R^{het} given in LLM are incorrect: for example at $S = 350$ we find SW solutions at $R = 1080$ and at $R = 1160$, whereas LLM report $R^{\mathrm{het}} = 1136$. At $R = 2100$ we observe a steady state. In contrast to LLM's results for $S = 350$ (their figure 5), the steady states we compute for periodic and constrained cases are the same.

If we take $L = 4$, so that the fundamental wavenumber is $k = \frac{1}{2}\pi$, the bifurcation diagram is as shown in figure 12. In particular there is a simultaneous Hopf bifurcation of the fundamental and is first harmonic ($k = \pi$) at $(S^{\mathrm{HH}}, R^{\mathrm{HH}}) \approx (1078.9, 1613.3)$. We have carried out simulations close to this double-Hopf point, at $S = 1089$ (so that $S - S^{\mathrm{HH}} \approx 10$); these are reported by Cox *et al.* (1992). We summarize the results here, and compare them with the simulations of LLM. There, as R is increased the first mode to become unstable is the $k = \pi$ mode, and weakly nonlinear theory predicts stable SW, which are indeed observed in numerical simulations of the partial differential equations. Then the weakly nonlinear theory predicts a thin wedge of parameters in which a mixed-mode two-frequency state is stable, composed of modes with wavenumbers $k = \frac{1}{2}\pi$ and $k = \pi$. This mixed mode is found in the numerical simulations, although this is a difficult search because the mixed mode at this finite distance from the double-Hopf point exists in a significantly smaller region of parameter space than would be projected based upon weakly nonlinear theory. For larger R, a pure $k = \frac{1}{2}\pi$ SW is predicted and observed, and finally at still larger R a $k = \frac{1}{2}\pi$ SS is computed. These results are in contrast to those of LLM, who describe integrations somewhat further from the double-Hopf point, at $S = 1200$. As they increase R, they first find stable SW with $k = \pi$, then a frequency-locked periodic solution involving both $k = \frac{1}{2}\pi$ and $k = \pi$ modes, then a quasi-periodic state analogous to our mixed modes, then a SW with $k = \frac{1}{2}\pi$, and finally an SS with $k = \frac{1}{2}\pi$. Thus their picture seems similar to ours, but their states are all reported to occur between the Hopf bifurcation lines of the $k = \frac{1}{2}\pi$ and $k = \pi$ modes in parameter space, whereas in fact our weakly nonlinear analysis and our numerical computations show, for example, that the two-frequency motions occur above both Hopf bifurcation lines.

We describe now our computations done at $S = 3000$ for a box with $L = 4$. (Here LLM found quasi-periodic, frequency-locked, and intermittently chaotic motions between $R = 3540$ and 3640, with these solution types appearing on one or the other

of two co-existing branches of solutions.) For $S = 3000$ the Hopf bifurcations to SW with wavenumbers $k = \pi$, $\frac{1}{2}\pi$ (called SW_π and $SW_{\pi/2}$) occur at $R = 3191.4$ and $R = 3827.4$ respectively, with frequencies $\omega_\pi = 19.80$ and $\omega_{\pi/2} = 4.88$. Our simulations were done by gradually increasing R with initial conditions that were a combination of π and $\frac{1}{2}\pi$ trigonometric modes. At $R = 3200$, we find only a π mode with $\omega = 19.94$ and $(Nu-1)_{\max,\min} = 0.0244, -0.001$. We compute this branch at $R = 3540$, 3630, 3815, 3835, 3900, 4100 and 4150. (We have been careful to investigate the stability of this branch to small disturbances with wavenumber $\frac{1}{2}\pi$, and it appears to be stable.) The angular frequency ω decreases slowly with increasing R, and at $R = 4150$, $\omega = 14.96$. The SW_π branch is stable at $R = 4150$ but has become unstable to perturbations with wavenumber $\frac{1}{2}\pi$ at $R = 4200$, giving rise to a second branch of solutions, with fundamental wavenumber $\frac{1}{2}\pi$. This second branch can be traced to $R = 3900$, 3835, 3815, 3700 and 3650. Its frequency is $\omega = 1.54$ at $R = 4200$, which decreases to $\omega = 1.17$ at $R = 3650$. This $\frac{1}{2}\pi$ state has significant contributions from π and its harmonics. A run started at $R = 3900$ with only $\frac{1}{2}\pi$ trigonometric disturbances develops into a $SW_{\pi/2}$ state with negligible π contributions and with $\omega = 4.22$, but which slowly becomes unstable to the aforementioned $\frac{1}{2}\pi$ state (with $\omega = 1.46$). As R increases, the contribution of π and its harmonics to this mode decreases. At $R = 4200$, $Nu-1$ for the SW varies in the small range between 3.05 and 3.10 over the cycle. At $R = 4250$ we find only a $\frac{1}{2}\pi$ SS with $Nu-1 = 3.17$. Thus the $\frac{1}{2}\pi$ and π states coexist between $R = 3650$ and $R = 4150$.

Appendix B. Simulation code

We follow the spectral approach of Moin & Kim (1980), originally developed for channel flows. This has been implemented and tested for both laminar and turbulent channel flow problems by Guang Yang (private communication), and our code is a modification of his version of the Moin & Kim code. The contributions due to the vortex force and the nonlinear terms in the momentum and energy equations are advanced in time by a second-order Adams–Bashforth method, pressure terms are advanced by a fully implicit scheme and viscous terms by a Crank–Nicholson method. The rotational (Lamb's) form of the momentum equations is used. Flow quantities are expressed in truncated Fourier–Chebyshev series, nonlinear terms are calculated pseudospectrally, and boundary conditions are enforced by the Lanczos tau method. To reduce the aliasing errors, we use the truncation strategy explained in Gilbert & Kleiser (1986).

Our modification to Yang's code adds an energy equation with Boussinesq approximation to the system of equations, and includes the 'vortex force' due to wave–current interaction in the momentum equations. Very general boundary conditions on top and bottom boundaries are also implemented, permitting the flexibility to simulate a variety of possible physical problems. Sidewalls can be chosen to be periodic or flux-free. In the latter case, θ, u and w are expanded in cosine series in the cross-stream direction (y), and v is expanded in a sine series. This forces the flux-free conditions.

In channel flow simulations done by Moin & Kim (1980) and Kim, Moin & Moser (1987), even and odd modes in the spectral space decouple. With the more general boundary conditions in our problem this is no longer so. As a consequence, the bandwidth of the matrix corresponding to each velocity for zero modes and normal vorticity and vertical velocity for non-zero modes is doubled. This necessitates a change in the way coefficients are computed and stored for each wavenumber pair in

	Nu	
R/R_c	PDE code	Moore & Weiss
6.0	3.58	3.58
10.0	4.35	4.38
15.0	5.07	5.06

TABLE 7. Comparison with Rayleigh–Bénard simulations of Moore & Weiss (1973), where their Prandtl number is $Pr = 1$. Here R_c is the critical value of the Rayleigh number for the onset of convection.

the homogeneous directions. Two possible options are specially tailored Gauss elimination (Canuto *et al.* 1987) or U–L factorization without pivoting (cf. Dennis & Quartapelle 1985). We instead employ a third alternative – an efficient blocking with computation time and storage comparable to the decoupled case. Optional pivoting may be used as well, though pivoting was found to be unnecessary in this case.

B.1. *Checks*

The modified spectral code has been subjected to various checks. First, we compare our results for the finite-amplitude, fully nonlinear Rayleigh–Bénard problem with those of Moore & Weiss (1973). There are two different ways to simulate this problem by distinct restrictions of our code, thereby enabling tests of two different parts of it. For example, the streamwise component of velocity may be identified with the negative perturbation temperature, $-\theta$, in the Rayleigh–Bénard problem. The x-direction of this problem is identified with the cross-stream $-y$ of LC. The destabilizing Rayleigh number R is Ra, the usual Rayleigh number in thermal convection, the Prandtl number is fixed at 1, and S is set to zero, obviating the need to deal with the energy equation. The boundary conditions on u in LC are thus no-slip and on v are stress-free conditions. The results agree well with Moore & Weiss (1973) at various values of Ra, as shown in table 7. This is a good check on a modified momentum equations and boundary conditions.

As a check on the energy equation, we can simulate the Rayleigh–Bénard problem alternatively by including the energy equation. To do this, we set $R = 0$, thereby removing the vortex force, and identify S to be $-Ra$, making it the destabilizing agent. The boundary conditions on u and v of LC are stress-free and θ is held fixed at top and bottom boundaries. Thus the LC problem reduces identically to the Rayleigh–Bénard problem. This check also shows excellent agreement with results of Moore & Weiss (1973).

As reported in §6, and by Cox *et al.* (1992), the results of the numerical simulations agree well with the weakly nonlinear analysis of this problem for periodic and flux-free lateral boundary conditions on the sidewalls for stress-free boundary conditions on the top and bottom of the layer.

Inspection of one-dimensional energy spectra in both the z- and y-directions provides a measure of the adequacy of the spatial resolution. With proper spatial resolution, the spectra should display exponential decay at the larger wavenumbers. The spatial resolution was found to be adequate with 16 Fourier modes in y and 17 Chebyshev modes in z, which is the resolution used in the calculations discussed in the paper. The Courant number for most runs was about 0.05 and was always less than 0.25. Computations were repeated with varied timestep sizes and spatial resolutions. Examples of spatial and temporal accuracy appear in table 8 and table 9

Resolution	$Nu-1$
8×17	4.0419
16×17	3.9619
32×17	3.9617

TABLE 8. Effect of spatial resolution on the Nusselt number, for the SS at $S = 350$, $R = 2100$. The first figure in the Resolution column indicates the number of Fourier modes taken in the y-direction, and the second indicates the number of Chebyshev modes in z.

Δt	ω
0.00050	5.815 ± 0.003
0.00125	5.82 ± 0.01
0.00250	5.82 ± 0.02

TABLE 9. Effect of different timesteps, Δt, on the frequency, ω, of the SW at $S = 350$, $R = 987$

respectively. For table 9 the frequency is computed by measuring the time elapsed between successive peaks of velocities sampled at various time intervals. This introduces an error corresponding to the sampling interval in time. The error bars refer to this source of error in the determination of the time period.

Appendix C. Algorithms for weakly nonlinear analysis

C.1. *Method of solution for non-degenerate operator* L

The governing equations for two-dimensional Langmuir circulations (with constant Stokes-drift gradient) are precisely those of double-diffusive convection: for ideal double diffusion, the weakly nonlinear analysis can be done exactly by hand, in particular the conditions of marginal stability are known exactly, as are the coefficients in the amplitude equations. For the LC problem this is not the case, because the boundary conditions are not as convenient as for IDD. To solve the linear stability problem for LC, and to carry out the weakly nonlinear calculations, we resort to numerical means. The z-structure of ψ, u and θ is expressed as an infinite sum of Chebyshev polynomials, which is truncated at some finite order for the numerical calculations. The boundary conditions were implemented by the tau method.

Thus any function $\boldsymbol{\Psi}(z)$ is represented in our finite Chebyshev truncation by a vector of coefficients. For example, if

$$\psi(z) = \sum_{i=1}^{N} \psi_i T_{i-1}(Z), \quad u(z) = \sum_{i=1}^{N} u_i T_{i-1}(Z), \quad \theta(z) = \sum_{i=1}^{N} \theta_i T_{i-1}(Z), \tag{C 1}$$

where $Z = 2z+1$, and $T_i(Z)$ is the ith Chebyshev polynomial, then $\boldsymbol{\Psi}(z)$ is represented in the numerical program by the vector of coefficients

$$\boldsymbol{\Psi} = (\psi_1, \ldots, \psi_N, \quad u_1, \ldots, u_N, \quad \theta_1, \ldots, \theta_N).$$

The operator $\partial/\partial Z$ is represented by an $N\times N$ matrix, $\mathbf{D}$, which, then applied to the vector of coefficients for $\psi(z)$, say, returns the vector of coefficients for $\partial\psi/\partial Z\,(= \frac{1}{2}\partial\psi/\partial z)$. Similarly the operation of multiplication by $h(z)$ is represented by a matrix $\mathbf{H}$ which acts on a coefficient vector for $u(z)$ and returns a coefficient vector for

$h(z)\,u(z)$. In setting up $\mathbf{H}$, we use (and truncate) the following identity (Abramowitz & Stegun 1965, p. 376), which expresses an exponential in terms of Chebyshev polynomials,

$$e^{\alpha Z} = I_0(\alpha) + 2\sum_{k=1}^{\infty} I_k(\alpha)\, T_k(Z), \tag{C 2}$$

where I_k is the modified Bessel function of order k.

Ignoring for the moment the boundary conditions on $z = 0, -1 (Z = \pm 1)$, we see that the linear eigenvalue problem to be solved for the growth rate σ is

$$\{\sigma \mathbf{J}(k) + \mathbf{K}_0(k)\}\, \hat{\boldsymbol{\Psi}} = \mathbf{0}, \tag{C 3}$$

where $\mathbf{J}(k)$ and $\mathbf{K}_0(k)$ are now $3N \times 3N$ matrices which represent the differential operators $\mathbf{J}$ and $\mathbf{K}_0$ of §2.2, with ∂_y replaced by ik. Thus

$$\mathbf{J}(k) = \begin{bmatrix} (4\mathbf{D}^2 - k^2\mathbf{I}) & 0 & 0 \\ 0 & \mathbf{I} & 0 \\ 0 & 0 & \mathbf{I} \end{bmatrix} \tag{C 4}$$

and

$$\mathbf{K}_0(k) = \begin{bmatrix} -(4\mathbf{D}^2 - k^2\mathbf{I})^2 & -ikR\mathbf{H} & ikS\mathbf{I} \\ -ik\mathbf{I} & -(4\mathbf{D}^2 - k^2\mathbf{I}) & 0 \\ -ik\mathbf{I} & 0 & -\tau(4\mathbf{D}^2 - k^2\mathbf{I}) \end{bmatrix}, \tag{C 5}$$

where $\mathbf{I}$ is the $N \times N$ identity matrix.

So far, from (C 3) the governing equation $\mathbf{L}(k)\, \hat{\boldsymbol{\Psi}} = \mathbf{0}$ for the eigenvector $\hat{\boldsymbol{\Psi}}$ is satisfied. Now we must apply the boundary conditions, using the tau method. There are four boundary conditions to be applied on $\hat{\psi}$, and rows $N-3$ to N of $\mathbf{J}(k)$ and $\mathbf{K}_0(k)$ are replaced by coefficients that encode these conditions. For example, with stress-free boundaries we want $\hat{\psi} = \hat{\psi}_{zz} = 0$ at $Z = \pm 1$. These boundary conditions give four independent linear equations to be satisfied by the coefficients $\{\psi_j\}_{j=1}^{N}$. These are

$$\psi_1 + \psi_2 + \ldots + \psi_N = 0 \quad (\psi = 0 \text{ on } Z = 1), \tag{C 6}$$

$$\psi_1 - \psi_2 + \ldots - (-1)^N \psi_N = 0 \quad (\psi = 0 \text{ on } Z = -1), \tag{C 7}$$

$$4\psi_3 + 24\psi_4 + \ldots + C_N = 0 \quad (\psi_{ZZ} = 0 \text{ on } Z = 1), \tag{C 8}$$

$$4\psi_3 - 24\psi_4 + \ldots - (-1)^N C_N = 0 \quad (\psi_{ZZ} = 0 \text{ on } Z = -1), \tag{C 9}$$

where $C_N = \frac{1}{3}(N-1)^2((N-1)^2 - 1)$.

To accommodate these conditions we replace rows $N-3$ to N of $\mathbf{K}_0(k)$ by the block

$$\left[\begin{array}{ccccc|c|c} 1 & 1 & 1 & \ldots & 1 & \multirow{4}{*}{$\mathbf{0}$} & \multirow{4}{*}{$\mathbf{0}$} \\ 1 & -1 & 1 & \ldots & -(-1)^N & & \\ 0 & 0 & 4 & \ldots & C_N & & \\ 0 & 0 & 4 & \ldots & -(-1)^N C_N & & \end{array}\right]. \tag{C 10}$$

The same rows of $\mathbf{J}$ are replaced by a $4 \times 3N$ matrix of zeros.

We apply a similar procedure for $\hat{u}$ and $\hat{\theta}$, but replacing just two rows in each case because there are two boundary conditions to be applied on each variable.

Let us now return to the eigenvalue problem (C 3). It is equivalent to

$$\mathbf{J}^{-1}(k)\, \mathbf{K}_0(k)\, \boldsymbol{\Psi} = -\sigma \boldsymbol{\Psi}, \tag{C 11}$$

so that $-\sigma$ is an eigenvalue of the matrix $\mathbf{J}^{-1}(k)\, \mathbf{K}_0(k)$. We have rewritten the generalized eigenvalue problem (C 3) as the standard eigenvalue problem (C 11). This

is immediate if $\mathbf{J}(k)$ is invertible, but here $\mathbf{J}(k)$ is not because it has eight zero rows. Nevertheless, the size of $\mathbf{J}(k)$, $\mathbf{K}_0(k)$ and $\boldsymbol{\Psi}$ can be reduced so that the reduced matrix, which we call $\mathbf{J}_s$, *is* invertible and then (C 11) makes sense. (The subscript s indicates that $\mathbf{J}_s$ has smaller dimensions than $\mathbf{J}(k)$.) The procedure is most easily explained when there is a single independent variable, ψ, say, rather than three, as in the LC problem. The generalization to three independent variables is conceptually straightforward, although the bookkeeping may require care.

Suppose that the eigenvalue problem for the single variable $\psi(z)$ is

$$(\sigma\mathbf{J}+\mathbf{K})\,\boldsymbol{\psi} = 0, \tag{C 12}$$

where $\boldsymbol{\psi} = (\psi_1, \psi_2, \ldots, \psi_N)$ is the vector of Chebyshev coefficients representing an approximation to $\psi(z)$, and that $\mathbf{J}$ and $\mathbf{K}$ are $N\times N$ matrices whose bottom M rows encode M boundary conditions on ψ. We partition $\mathbf{J}$, $\mathbf{K}$ and $\boldsymbol{\psi}$ as follows:

$$\mathbf{J} = \begin{bmatrix} \mathbf{J}_1 & \mathbf{J}_2 \\ \mathbf{J}_3 & \mathbf{J}_4 \end{bmatrix}, \quad \mathbf{K} = \begin{bmatrix} \mathbf{K}_1 & \mathbf{K}_2 \\ \mathbf{K}_3 & \mathbf{K}_4 \end{bmatrix}, \quad \boldsymbol{\psi} = \begin{bmatrix} \boldsymbol{\psi}_1 \\ \boldsymbol{\psi}_2 \end{bmatrix}. \tag{C 13}$$

Here $\mathbf{J}_1$ and $\mathbf{J}_2$ have $N-M$ rows, and $\mathbf{J}_3$ and $\mathbf{J}_4$ have M rows. $\mathbf{J}_1$ and $\mathbf{J}_3$ have $N-M$ columns, and $\mathbf{J}_2$ and $\mathbf{J}_4$ have M columns. (Similarly for $\mathbf{K}$.) $\boldsymbol{\psi}_1$ has $N-M$ rows, and $\boldsymbol{\psi}_2$ has M rows.

The M boundary conditions are expressed by the last M rows of the matrix equation (C 12), and these are

$$\mathbf{K}_3\boldsymbol{\psi}_1+\mathbf{K}_4\boldsymbol{\psi}_2 = -\sigma(\mathbf{J}_3\boldsymbol{\psi}_1+\mathbf{J}_4\boldsymbol{\psi}_2) = \mathbf{0}, \tag{C 14}$$

where the last equality holds because $\mathbf{J}_3 = \mathbf{J}_4 = \mathbf{0}$. Therefore

$$\boldsymbol{\psi}_2 = -\mathbf{K}_4^{-1}\mathbf{K}_3\boldsymbol{\psi}_1. \tag{C 15}$$

($\mathbf{K}_4$ is invertible provided the boundary conditions are independent, and provided they do not involve derivatives of $\psi(z)$ of higher order than $(N-1)$ – this last point because of the finite Chebyshev truncation.)

The governing equation for $\psi(z)$ is described by the first $N-M$ rows of (C 12), which are

$$\mathbf{K}_1\boldsymbol{\psi}_1+\mathbf{K}_2\boldsymbol{\psi}_2 = -\sigma(\mathbf{J}_1\boldsymbol{\psi}_1+\mathbf{J}_2\boldsymbol{\psi}_2), \tag{C 16}$$

and using (C 15) to substitute for $\boldsymbol{\psi}_2$ in terms of $\boldsymbol{\psi}_1$, these become

$$(\mathbf{K}_1-\mathbf{K}_2\mathbf{K}_4^{-1}\mathbf{K}_3)\,\boldsymbol{\psi}_1 = -\sigma(\mathbf{J}_1-\mathbf{J}_2\mathbf{K}_4^{-1}\mathbf{K}_3)\,\boldsymbol{\psi}_1.$$

In general the $(N-M)$-square matrices $\mathbf{K}_s \equiv \mathbf{K}_1-\mathbf{K}_2\mathbf{K}_4^{-1}\mathbf{K}_3$ and $\mathbf{J}_s \equiv \mathbf{J}_1-\mathbf{J}_2\mathbf{K}_4^{-1}\mathbf{K}_3$ have full rank. Thus we have the standard eigenvalue problem

$$\mathbf{J}_s^{-1}\mathbf{K}_s\boldsymbol{\psi}_1 = -\sigma\boldsymbol{\psi}_1, \tag{C 17}$$

which can readily be solved in a computer algebra package such as Mathematica. A by-product of the solution is the following decomposition,

$$\mathbf{J}_s^{-1}\mathbf{K}_s = \mathbf{V}^{\mathrm{T}}\boldsymbol{\Lambda}(\mathbf{V}^{\mathrm{T}})^{-1}, \tag{C 18}$$

where $\boldsymbol{\Lambda} = \mathrm{diag}[-\sigma_1, \ldots, -\sigma_{N-M}]$, $-\boldsymbol{\Lambda}$ is the diagonal matrix of eigenvalues of (C 12), and $\mathbf{V}$ is a matrix whose rows are the corresponding eigenvectors.

The reduction to be applied to the matrices $\mathbf{J}$ and $\mathbf{K}$ that arise in the LC problem is slightly more complicated. Each of the vectors representing the Chebyshev coefficients of the three variables is split into two parts, and each of the nine blocks that comprise $\mathbf{J}$ and $\mathbf{K}$ is split into four sub-blocks. This requires careful bookkeeping.

Most of the calculations involved in the weakly nonlinear analysis are carried out on the reduced vectors analogous to $\boldsymbol{\psi}_1$ since the extra elements analogous to $\boldsymbol{\psi}_2$ can be inferred from equations like (C 15). The exception is in the calculation of the Jacobian, where we use the full vectors to calculate the nonlinear interactions in spectral space. In what follows we drop the subscript s on the reduced matrices, for clarity of notation.

At $O(\epsilon^2)$, equations like

$$\{n_1 \mathrm{i}\omega \mathbf{J}(n_2 k) + \mathbf{K}_0(n_2 k)\}\, \boldsymbol{\Psi}_2^{(n_1, n_2)} = \boldsymbol{R}_2^{(n_1, n_2)}, \tag{C 19}$$

must be solved, where $\boldsymbol{R}_2^{(n_1, n_2)}$ denotes the quadratic nonlinear terms from $\mathbf{N}(\boldsymbol{\Psi}_1, \boldsymbol{\Psi}_1)$ which are proportional to $\mathrm{e}^{n_2 \mathrm{i}ky + n_1 \mathrm{i}\omega t}$. The matrices $\mathbf{L}(n_1, n_2) = n_1 \mathrm{i}\omega \mathbf{J}(n_2 k) + \mathbf{K}_0(n_2 k)$ can easily be calculated, and then inverted to give $\boldsymbol{\Psi}_2^{(n_1, n_2)} = \mathbf{L}^{-1}(n_1, n_2)\, \boldsymbol{R}_2^{(n_1, n_2)}$.

There is a subtlety in the calculation of $\boldsymbol{\Psi}_2^{(0,0)}$ when flux-free boundary conditions are applied. The matrix $\mathbf{L}(0,0)$ is singular because the boundary conditions $u_Z = 0$ at $Z = \pm 1$ allow an arbitrary multiple of the complementary function

$$(\hat{\psi}, \hat{u}, \hat{\theta}) = (0, 1(Z), 0)$$

to be added to $\boldsymbol{\Psi}_2^{(0,0)}$. More precisely, if $\boldsymbol{\Psi}_2^{(0,0)} = (\hat{\psi}, \hat{u}, \hat{\theta})$ solves $\mathbf{L}(0,0)\, \boldsymbol{\Psi}_2^{(0,0)} = \boldsymbol{R}_2^{(0,0)}$, then so does $\hat{\boldsymbol{\Psi}}_2^{(0,0)} = (\hat{\psi}, \hat{u} + a, \hat{\theta})$ for any constant a. In terms of the matrix $\mathbf{L}(0,0)$ the ambiguity arises as follows.

$\mathbf{L}(0,0)$ is composed of three blocks that sit on its leading diagonal, $\mathbf{L}(0,0) = \mathrm{diag}\,[\mathbf{L}_1, \mathbf{L}_2, \mathbf{L}_3]$. The first column of $\mathbf{L}_2$ is zero because (i) the equations depend only on u_{ZZ} but not on u_Z or u, so the first two columns of the equation rows vanish, and (ii) the stress-free boundary conditions depend only on u_Z so the first column of the boundary condition rows vanishes. Therefore $\mathbf{L}_2$ is a singular matrix, and its top row is a linear combination of its other rows. We replace the top row by the row $[1, 0, 0, \ldots, 0]$, which fixes the vector of Chebyshev coefficients u_i to have zero as a first element. This procedure makes no difference to the calculations at any order because only derivatives of u with respect to y, Z or t occur in the governing equations and in the boundary conditions. Choosing a different first element is equivalent to making a Galilean transformation.

Once the terms of $O(\epsilon^2)$ are calculated then attention turns to the third-order problem, and the calculation of the amplitude equation(s). The resonant nonlinear terms are selected – these are the terms proportional to $\mathrm{e}^{\mathrm{i}ky + \mathrm{i}\omega t}$ with the z-structure of the marginal eigenfunction. The equation to be satisfied by the cubic term proportional to $\mathrm{e}^{\mathrm{i}ky + \mathrm{i}\omega t}$ is

$$\{\mathrm{i}\omega \mathbf{J}(k) + \mathbf{K}_0(k)\}\, \boldsymbol{\Psi}_3^{(1,1)} = \boldsymbol{R}_3^{(1,1)}. \tag{C 20}$$

But we know that $\mathbf{J}^{-1}\mathbf{K}_0 = \mathbf{V}^{\mathrm{T}} \boldsymbol{\Lambda} (\mathbf{V}^{\mathrm{T}})^{-1}$, so

$$\{\mathrm{i}\omega \mathbf{I} + \mathbf{V}^{\mathrm{T}} \boldsymbol{\Lambda} (\mathbf{V}^{\mathrm{T}})^{-1}\}\, \boldsymbol{\Psi}_3^{(1,1)} = \mathbf{J}^{-1} \mathbf{R}_3^{(1,1)},$$

and therefore

$$\{\mathrm{i}\omega \mathbf{I} + \boldsymbol{\Lambda}\}\, (\mathbf{V}^{\mathrm{T}})^{-1}\, \boldsymbol{\Psi}_3^{(1,1)} = (\mathbf{V}^{\mathrm{T}})^{-1}\, \mathbf{J}^{-1} \boldsymbol{R}_3^{(1,1)}.$$

Since $\mathrm{i}\omega$ is one of the eigenvalues already found numerically then some diagonal element of $\mathrm{i}\omega \mathbf{I} + \boldsymbol{\Lambda}$ is zero, the mth element, say. (*Mathematica* does not necessarily sort the eigenvalues in the order of their real parts.) Therefore the corresponding mth element of $(\mathbf{V}^{\mathrm{T}})^{-1} \mathbf{J}^{-1} \boldsymbol{R}_3^{(1,1)}$ must vanish also. If we are considering a steady bifurcation then $\omega = 0$, and since $\boldsymbol{R}_3^{(1,1)}$ includes terms like A, $A|A|^2$ and $\mathrm{d}A/\mathrm{d}T$, then we arrive at the evolution for A by insisting that a given element of $(\mathbf{V}^{\mathrm{T}})^{-1} \mathbf{J}^{-1} \boldsymbol{R}_3^{(1,1)}$ should vanish. If we are considering a Hopf bifurcation then $\omega \neq 0$, and there are two

N	R^{HH}	S^{HH}
10	1613.5596	1079.0931
12	1613.3038	1078.8753
14	1613.3066	1078.8779
16	1613.3066	1078.8779

TABLE 10. (R^{HH}, S^{HH}) is the computed location of the multiple Hopf bifurcation involving the $k = \frac{1}{2}\pi$ and $k = \pi$ modes, when $L = 4$ and $\lambda = 0$. The number of Chebyshev polynomials used for each of $\hat{\psi}$, $\hat{u}$ and $\hat{\theta}$ is N.

amplitudes; A_1 of the left-TW, and A_2 of the right-TW. In this case $\boldsymbol{R}_3^{(1,1)}$ includes terms like A_1, $A_1|A_1|^2$, $A_1|A_2|^2$ and $\mathrm{d}A_1/\mathrm{d}T$, and we obtain an evolution equation for A_1. The evolution equation for A_2 is just the complex conjugate of the evolution equation for A_1, with $(A_1, A_2) \mapsto (A_2, A_1)$.

This derivation of the amplitude equation(s) by algebraic manipulation of (C 20) is mathematically equivalent to requiring that the inner product of (C 20) with the adjoint eigenfunction $\boldsymbol{\Psi}^\dagger$ be satisfied. For $\boldsymbol{\Psi}^\dagger\{\mathrm{i}\omega\mathbf{J} + \mathbf{K}_0\} = \mathbf{0}$ implies that $\boldsymbol{\Psi}^\dagger\mathbf{J}\{\mathrm{i}\omega\mathbf{I} + \mathbf{V}^{\mathrm{T}}\boldsymbol{\Lambda}(\mathbf{V}^{\mathrm{T}})^{-1}\} = \mathbf{0}$, and so $\boldsymbol{\Psi}^\dagger\mathbf{J}\mathbf{V}^{\mathrm{T}}\{\mathrm{i}\omega\mathbf{I} + \boldsymbol{\Lambda}\} = \mathbf{0}$. But the mth column of $\mathrm{i}\omega\mathbf{I} + \boldsymbol{\Lambda}$ is zero, because $\sigma_m = -\mathrm{i}\omega$, and so $\boldsymbol{\Psi}^\dagger\mathbf{J}\mathbf{V}^{\mathrm{T}} = \boldsymbol{E}_m$, where $\boldsymbol{E}_m$ is the row vector whose mth element is one and whose other elements are zero. Therefore, $\boldsymbol{\Psi}^\dagger = \boldsymbol{E}_m(\mathbf{V}^{\mathrm{T}})^{-1}\mathbf{J}^{-1}$, and $\boldsymbol{\Psi}^\dagger$ is the mth row of $(\mathbf{V}^{\mathrm{T}})^{-1}\mathbf{J}^{-1}$. So the mth row of $(\mathbf{V}^{\mathrm{T}})^{-1}\mathbf{J}^{-1}\boldsymbol{R}_3^{(1,1)}$ equals the inner product of $\boldsymbol{R}_3^{(1,1)}$ and $\boldsymbol{\Psi}^\dagger$.

We have checked that the matrix method for determining the solvability condition gives results in agreement with the direct computation of the adjoint solution, and the explicit evaluation of the inner products in (18). The numerical values of the coefficients in the amplitude equations computed by the two different methods agree to within a small numerical tolerance. (For the cases we have computed the agreement is to five or six significant figures.)

C.2. *Method of solution for degenerate operator* $\mathbf{L}$

If the linear operator $\mathbf{L}$ has a degenerate eigenspace then we cannot use the decomposition of the previous section to compute the solvability condition. Instead we use the singular value decomposition. In practice the difference is that the singular value decomposition yields

$$\mathbf{J}^{-1}(k)\,\mathbf{K}_0(k) = \mathbf{U}^{\mathrm{T}}\boldsymbol{\Lambda}\mathbf{V}, \tag{C 21}$$

where $\boldsymbol{\Lambda}$ is the diagonal matrix of singular values, and for the case we are considering the last element of $\boldsymbol{\Lambda}$ is zero (or at least to within numerical tolerance). The computer algebra calculations mirror the operator calculations described in §3.3.

C.3. *Accuracy of finite Chebyshev truncation*

For ideal double diffusion the z-structure of each term in the expansion of $\boldsymbol{\Psi}$ can be described exactly by a sine or cosine. For LC the z-structure is more complicated – the finite truncation of Chebyshev polynomials leads to a truncation error. This error is particularly important for large values of λ, where the Stokes-drift gradient, $h(z) = \mathrm{e}^{2\lambda z}$, is non-zero in a thin boundary layer near $z = 0$, and approximately zero elsewhere. Table 10 shows as an example the convergence of the computed values of (R^{HH}, S^{HH}) (the point where $\mathbf{L}$ has two pairs of imaginary eigenvalues, one pair each for the modes with $k = \frac{1}{2}\pi$ and π, when the domain has length $L = 4$) as N, the number of polynomials used for each of $\hat{\psi}$, $\hat{u}$ and $\hat{\theta}$, is increased. In this case $\lambda = 0$.

	$(Nu_S-1)/(R_T-R_1)$	
	Weakly nonlinear analysis	Huppert & Moore (1976)
(*a*)	$0.005982(1+1.1842\sin 2p_0t)$	$0.005984(1+1.1842\sin 2p_0t)$
(*b*)	$0.009312(1+0.1676\sin 2p_0t)$	$0.009310(1+0.1676\sin 2p_0t)$

TABLE 11. Comparison with analysis by Huppert & Moore (1976). All symbols are in their notation for an ideal double diffusion problem with $\alpha = 2^{-\frac{1}{2}}$, $\sigma = 1$. For case (*a*) $R_S = 100$, $\tau = 1/6.7$ and computed $R_1 = 925.8933$, $p_0 = 3.04905$ by both methods. For case (*b*), $R_S = 5000$, $\tau = 0.1$ and computed $R_1 = 3545.56$, $p_0 = 27.3463$ by both methods.

We have used $N = 10$ for preliminary investigations to decide, for example, whether a particular coefficient is positive or negative. For the calculation of definite values of the coefficients we have generally used $N = 14$.

C.4. *Checks on the weakly nonlinear computations*

The coefficients we calculate have been checked in several ways. First, they have been checked against the analytical linear and weakly nonlinear results given by Huppert & Moore (1976) for ideal double diffusion. They consider a Hopf bifurcation with flux-free boundary conditions, so the solution is forced to be a SW. Thus it is possible to check α and β only in combinations $\alpha_r+\beta_r$ and $\alpha_i+\beta_i$. These agree well; the Nusselt numbers calculated by the weakly nonlinear analysis is compared in table 11 with that constructed from equations (4.5) and (4.7) of the Huppert & Moore paper.

Secondly, we have extended the perturbation analysis done by Huppert & Moore to include periodic boundary conditions. The weakly nonlinear analysis in this case can again be done analytically, and incorporates $O(2)$ symmetry, thereby including both standing and travelling waves. We find that all details of the analytical and numerical computations to the same level of accuracy found in table 11. This is a strong check on both the structure of the computer algebra code, and on its details. Thirdly, independent numerical calculations of the coefficients have been made by Tom Allen (private communication), using a different program, and he has notified us that his results agree with ours.

REFERENCES

ABRAMOWITZ, M. & STEGUN, I. A. 1965 *Handbook of Mathematical Functions*. Dover.

BRETHERTON, C. S. & SPIEGEL, E. A. 1983 Intermittency through modulational instability. *Phys. Lett.* A **96**, 152–156.

CANUTO, C., HUSSAINI, M. Y., QUARTERONI, A. & ZANG, T. A. 1987 *Spectral Methods in Fluid Dynamics*. Springer.

COX, S. M. & LEIBOVICH, S. 1992 Langmuir circulations in a surface layer bounded by a strong thermocline. *J. Phys. Oceanogr.* (submitted).

COX, S. M., LEIBOVICH, S., MOROZ, I. M. & TANDON, A. 1992 Hopf bifurcations with $O(2)$ symmetry in Langmuir circulations. *Physica* D (submitted).

CRAIK, A. D. D. 1977 The generation of Langmuir circulations by an instability mechanism. *J. Fluid Mech.* **81**, 209–223.

CRAIK, A. D. D. & LEIBOVICH, S. 1976 A rational model for Langmuir circulations. *J. Fluid Mech.* **73**, 401–426.

DANGELMAYR, G. & KNOBLOCH, E. 1986 Interaction between standing and travelling waves and steady states in magnetoconvection. *Phys. Lett.* A 117, 394–398.

DANGELMAYR, G. & KNOBLOCH, E. 1987 The Takens–Bogdanov bifurcation with $O(2)$-symmetry. *Phil. Trans. R. Soc. Lond.* A **322**, 243–279.

DEANE, A. E., KNOBLOCH, E. & TOOMRE, J. 1987 Traveling waves and chaos in thermosolutal convection. *Phys. Rev.* A **36**, 2862–2869.

DENNIS, S. C. R. & QUARTAPELLE, L. 1985 Spectral algorithms for vector elliptic equations in a spherical gap. *J. Comput. Phys.* **61**, 218–241.

GILBERT, N. & KLEISER, L. 1986 Subcritical transition to turbulence in channel flow. In *Direct and Large Eddy Simulation of Turbulence* (ed. U. Schumann & R. Friedrich) , pp. 1–18. Vieweg.

HUPPERT, H. E. & MOORE, D. R. 1976 Nonlinear double-diffusive convection. *J. Fluid Mech.* **78**, 821–852.

KIM, J., MOIN, P. & MOSER, R. 1987 Turbulence statistics in fully developed channel flow at low Reynolds number. *J. Fluid Mech.* **177**, 133–166.

KNOBLOCH, E. 1985 Doubly diffusive waves. In *Double Diffusive Motions* (ed. N. E. Bixler & E. Spiegel), FED vol. 24, pp. 17–22. ASME.

KNOBLOCH, E. 1986 Oscillatory convection in binary mixtures. *Phys. Rev.* A **34**, 1538–1549.

KNOBLOCH, E., DEANE, A. E. & TOOMRE, J. 1987 Oscillatory double diffusive convection: theory and experiment. In *The Physics of Structure Formation: Theory and Simulation* (ed. W. Güttinger & G. Dangelmayr), pp. 117–129. Springer.

KNOBLOCH, E. & MOORE, D. R. 1990*a* Minimal model of binary convection. *Phys. Rev.* A **42**, 4693–4709.

KNOBLOCH, E. & MOORE, D. R. 1990*b* Nonlinear convection in binary mixtures. In *Nonlinear Evolution of Spatio-Temporal Structures in Dissipative Continuous Systems* (ed. F. H. Busse & L. Kramer), pp. 109–129. Springer.

LANGMUIR, I. 1938 Surface motion of water induced by wind. *Science* **87**, 119–123.

LEIBOVICH, S. 1977*a* On the evolution of the system of wind drift currents and Langmuir circulations in the ocean. Part 1. Theory and averaged current. *J. Fluid Mech.* **79**, 715–743.

LEIBOVICH, S. 1977*b* Convective instability of stably stratified water in the ocean. *J. Fluid Mech.* **82**, 561–581.

LEIBOVICH, S. 1980 On wave–current interaction theories of Langmuir circulations. *J. Fluid Mech.* **99**, 715–724.

LEIBOVICH, S. 1983 The form and dynamics of Langmuir circulations. *Ann. Rev. Fluid Mech.* **15**, 391–427.

LEIBOVICH, S. 1985 Dynamics of Langmuir circulations in a stratified ocean. In *The Ocean Surface* (ed. Y. Toba & H. Mitsuyasu), pp. 457–464. Reidel.

LEIBOVICH, S., LELE, S. K. & MOROZ, I. M. 1989 Nonlinear dynamics in Langmuir circulations and in thermosolutal convection. *J. Fluid Mech.* **198**, 471–511 (referred to herein as LLM).

LELE, S. K. 1985 Some problems in hydrodynamic stability arising in geophysical fluid dynamics. Ph.D. thesis, Cornell University, 302 pp.

MAHALOV, A. & LEIBOVICH, S. 1991*a* On the calculation of coupling coefficients in amplitude equations. *J. Comput. Phys.* In press.

MAHALOV, A. & LEIBOVICH, S. 1991*b* Multiple bifurcations of rotating pipe flow. *Theor. Comput. Fluid Mech.* In press.

MOIN, P. & KIM, J. 1980 On the numerical solution of time-dependent viscous incompressible fluid flows involving solid boundaries. *J. Comput. Phys.* **35**, 381–392.

MOORE, D. R. & WEISS, N. O. 1973 Two-dimensional Rayleigh–Bénard convection. *J. Fluid Mech.* **58**, 289–312.

MOROZ, I. M. & LEIBOVICH, S. 1985 Competing instabilities in a nonlinear model for Langmuir circulations. *Phys. Fluids* **28**, 2050–2061.

NIELD, D. A. 1967 The thermohaline Rayleigh–Jeffreys problem. *J. Fluid Mech.* **29**, 545–558.

RUBENFELD, L. A. 1978 On a derivative expansion technique, and some comments on multiple scaling in the asymptotic approximation of solutions of certain differential equations. *SIAM Rev.* **20**, 78–105.